In Situ Spectroscopic Studies of Cysteine Adsorbed on Silver Electrodes

By

Simon David Peter Birnie-Lefcovitch
B.Sc., Acadia University, 2006

A Thesis Submitted in Partial Fulfillment
of the Requirements for the Degree of

MASTER OF SCIENCE

in the Department of Chemistry

University of Victoria

In Situ Spectroscopic Studies of Cysteine Adsorbed on Silver Electrodes

By

Simon David Peter Birnie-Lefcovitch
B.Sc., Acadia University, 2006

Supervisory Committee

Dr. Alexandre G. Brolo, Supervisor
(Department of Chemistry)

Dr. David A. Harrington, Departmental Member
(Department of Chemistry)

Dr. Dennis K. Hore, Departmental Member
(Department of Chemistry)

Abstract

Supervisory Committee

Dr. Alexandre G. Brolo, Supervisor
(Department of Chemistry)

Dr. David A. Harrington, Departmental Member
(Department of Chemistry)

Dr. Dennis K. Hore, Departmental Member
(Department of Chemistry)

The study of interfacial processes has long been of interest to scientists. The properties of a material are generally governed by the characteristics of its surface, thus the development of surface specific experimental methods are always of great importance to the scientific community. This thesis presents the results of the spectroelectrochemical characterization of a cysteine-Ag adsorbate-substrate system. The system was probed using two spectroelectrochemical methods.

The chiral effect which cysteine has on the electronic structure of the Ag substrate was studied by performing *in situ* second harmonic generation optical rotatory dispersion (SHG-ORD) experiments. Rotation angles (ϕ) obtained indicated that the overlayers of adsorbed cysteine molecules imprinted the electronic structure of the Ag with their inherent optical activity. Results also indicate that there are one or more other processes which are contributing to the observed ϕ values.

The second half of this thesis discusses the effect that pH and applied potential have on the adsorption geometry of L-cysteine on polycrystalline Ag as studied by

surface enhanced Raman scattering (SERS). Results obtained under neutral and acidic conditions showed that the coadsorption of Cl^- plays an important role in the adsorption geometry. At more positive potentials Cl^- will be coadsorbed on the Ag surface with cysteine. The Cl^- helps to stabilize the adsorbed cysteine *via* interactions with the protonated amino group. Consequently, as the potential is changed in the cathodic direction the Cl^- becomes desorbed from the surface, resulting in changing intensities observed in the SERS spectra. Tracking of which peaks, and consequently vibrational modes, are changing and in which way allowed for a qualitative determination of the adsorption geometry as a function of both pH and potential.

Table of Contents

List of Figures

Acknowledgments

The completion of this Master's thesis has been an incredible journey for me, and there are many people who I have to thank for making this entire experience more fulfilling, rewarding and enjoyable. As with all major endeavours which I have chosen to undertake in my life I owe many thanks to my family in the completion of this task. My parents, Vurla and Shelly, and my sister, Anna, have always provided me with unconditional support and insightful guidance, and for that I am very grateful. I would not be the person I am today without them, and I hope they take that as a compliment. I must also recognize the efforts of my girlfriend Jenn. You have been extremely patient with me but we have made it through now and have new adventures to look forward to.

Since coming to Victoria I have been fortunate to have had many friends and colleagues who have shared in my triumphs, failures and the happenings of everyday life. Whether grad student, faculty or teaching staff you have made my time here much more than just an education. I would especially like to thank Nichole and Jane for their upbeat attitude and dedication. The interest you take in your TAs and your students is noticed and most certainly appreciated.

I would also like to thank Jean-Paul and Doug in the mechanical shop and Sean in the glass shop. I'm not sure what I would have done if you had not been there to fix all of the things I broke.

The Brolo group has changed quite a bit since I first joined, however the interesting personalities and helpful mindset of all group members past and present has made for the best research group one could hope for. To my Brazilian friends, Marcos and Gustavo, thank you for many helpful discussions about research, Canada and Brazil. I will make it to Fernando de Noronha eventually! To Claire, one of our summer students, thank you for you invaluable contribution to the SERS experiments. I would also like to thank Aaron Sanderson for teaching me everything I needed to know about SHG and for his contributions to the data. You always added a delightful touch of unpredictability to any scientific discussion, so thank you for keeping me on my toes.

Finally, and most importantly I would like to thank my supervisor Dr. Alex Brolo. I have never met a harder working person nor someone more knowledgeable in everything related to spectroscopy. Most importantly I want to acknowledge your patience and helpfulness in all our exchanges. You have always been approachable for help when it was needed and provided an intellectually stimulating and supportive environment for my graduate education.

Chapter 1 - Introduction

1.1 Motivation

The surfaces of materials are often responsible for many of the properties which they exhibit. This makes understanding the behaviour of surfaces and interfaces one of the most important branches of research in modern chemistry. Areas of research such as catalysis, biosensing, and fuel cells, among many others, rely heavily on fast and descriptive methods which can be used to characterize surfaces.

Second harmonic generation (SHG) and surface enhance Raman scattering (SERS) are techniques which can offer a wealth of information on surface processes. They are both highly surface sensitive, and well adapted to the study of *in situ* electrode surfaces. They complement each other quite well, with SERS providing the researcher with a look at the vibrational characteristics of the adsorbates and how the metal is interacting with them. Conversely, SHG contributes information about the electronic structure of the electrode itself and how it has been affected by the adsorbates which are attached to it.

The system being studied consists of cysteine adsorbed onto a polycrystalline Ag electrode. This system has several advantages which led to its use in the study presented in this thesis. The electrons in Ag are easily perturbed which allows for both SERS and SHG experiments to be performed with strong signal strength. Despite Ag being the best metal for inducing a SERS enhancement, it has not been studied as extensively as Au, due to the fact that it oxidizes in air. The chemistry of

Ag is very similar to that of Au however, thus we are able to use the many studies performed on Au to model the behaviour of Ag. The use of cysteine also provides many advantages, which are enumerated throughout the thesis. There are three main reasons cysteine was chosen for these studies however. First, it is an amino acid. This means that it has several applications such as the modeling of protein-protein interactions[1]. Second, cysteine has multiple functional groups. These varied functionalities imbue cysteine with a broad and varied chemistry, allowing it to interact with many different species. This property makes it an ideal linker for immobilizing analytes of interest, particularly biological compounds. Finally, cysteine is a small molecule, which should result in simplifying the interpretation of results.

Studies geared towards the fundamental understanding of the processes which occur at interfaces have been of interest for a long time, however there is still much to be contributed to the field, and many more advances to be discovered. This investigation is aimed principally at increasing the fundamental knowledge base of metal-adsorbate interactions, and the methods by which they can be examined.

1.2 Organization of the Thesis

This thesis is divided into four chapters including this first introduction chapter. In Chapter 1 background knowledge pertinent to the experiments conducted will be presented to provide the reader with the ability to understand and interpret the experimental results. The first section is dedicated to the amino acid cysteine, the

molecule which was used to functionalize the Ag surface studied. The remainder and bulk of the introduction reviews the fundamental theory of the experimental techniques used, providing an overview of second harmonic generation (SHG), Raman scattering, surface enhanced Raman scattering (SERS) and *ab initio* calculations. This chapter equips the reader with the tools necessary to comprehend the interpretations presented in the second and third chapters where the experimental results are discussed.

Each of the results chapters is a self-contained report, consisting of the sections generally found in a journal article. An introduction outlining important theory development specific to the experiments conducted and summarizing the knowledge already established within the scientific community opens each results chapter. This is meant to build upon the theory discussed in Chapter 1 and focus in on the specific experiments being discussed. This is followed by an experimental section where the experimental set-up and parameters are laid out. Results are then presented and discussed, and the insights and conclusions gained are summarized in a final section.

A final short chapter discusses the relationship between the results obtained in Chapter 2 and Chapter 3 and how they relate to each other. References for all chapters are located directly after Chapter 4.

1.3 Cysteine

Cysteine is one of the 20 natural amino acids used in the forming of proteins. It can further be classified as a “non-essential” amino acid because it is produced in the human body and does not need to be obtained from external sources such as food. Its functionality consists of the amino and carboxylic acid groups, common to all amino acids, with a thiol group side chain (Figure 1.1(a)). Cysteine is easily dimerized to cystine by oxidization of the thiol group to form a disulfide bond (Figure 1.1(b)). This process is most likely to occur under neutral or basic conditions[2]. These rigid disulfide bonds are important to maintain the structure of proteins such as keratin in hair.

Cysteine has a chiral centre at the α-carbon and thus can exist as either the D or L enantiomer, though only L-cysteine is found naturally.

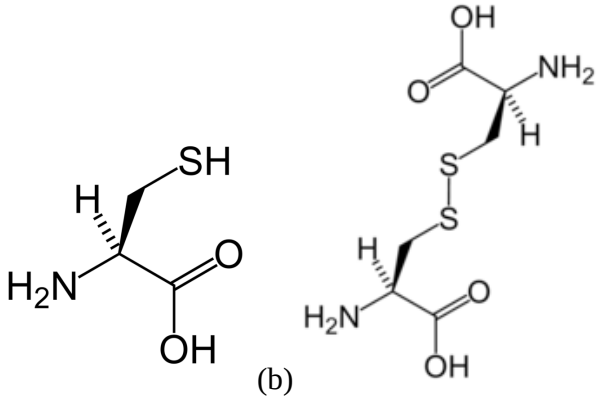

(a) (b)

Figure 1.1 - Molecular structure of (a) L-cysteine and (b) L-cystine.

1.3.1 Protonation of Cysteine

Cysteine is a small molecule, having a molar mass of only 121.16 g/mol and is highly soluble in water[2] due to its high polarity. The three functional groups of cysteine all undergo protonation/deprotonation in aqueous media, leading to several forms of cysteine which are ionized to varying degrees as pH changes. Each of these functional groups has a pK_a associated with it, 1.91, 8.16 and 10.25 for the carboxyl, amino and thiol groups respectively[3]. Using these values to determine the fraction of each form of cysteine (α) at a pH value provides a graphical representation of the degree of protonation of cysteine as a function of pH (Figure 1.2). It is clear from Figure 1.2 that under neutral conditions (pH=7) cysteine exists predominantly in its zwitterionic form with the amine protonated and the carboxylic acid deprotonated. At low pH cysteine is fully protonated, however the protonation is not as clear cut at higher pH values. The acid strength of the thiol and amino groups are about the same, therefore making it unclear which species is actually dominant until $pH>pK_{a3}$ where cysteine is fully deprotonated.

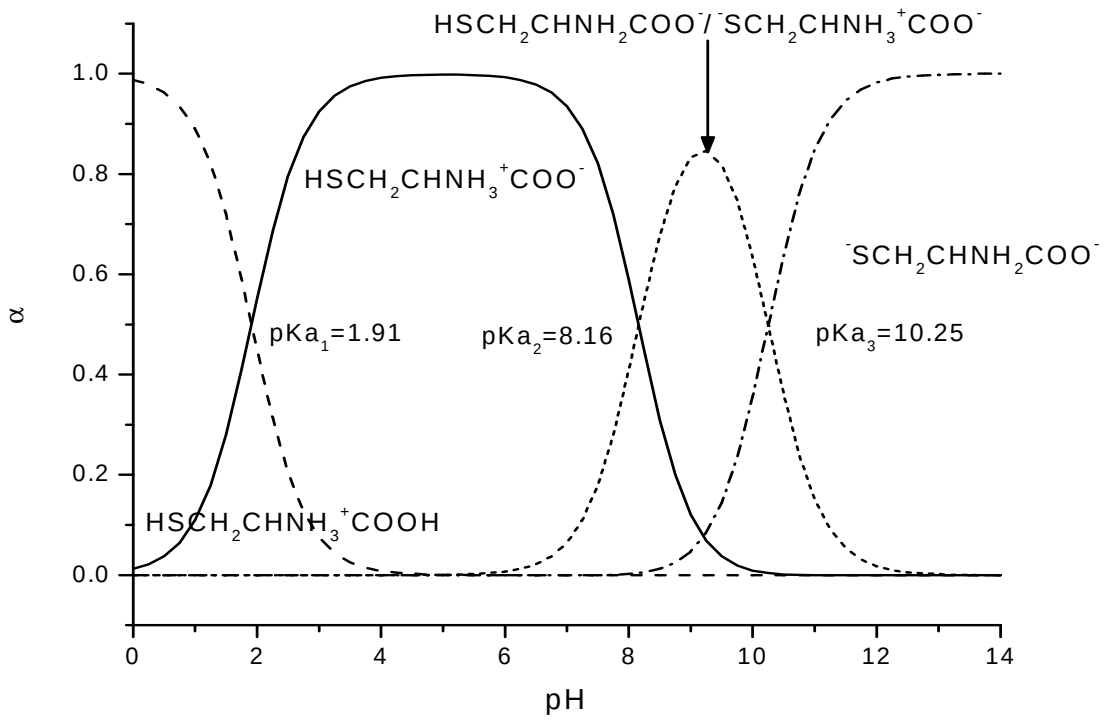

Figure 1.2 - Degree of protonation of cysteine as a function of pH

1.3.2 Synthesis of L-Cysteine

There are several chemical synthesis pathways to produce L-cysteine, such as that put forth by Martens *et al.* in 1981[4]. They have the downside of producing a racemic mixture which must then be further purified to separate the enantiomers from each other. This is not practical for large scale manufacturing of the compound. Reduction of L-cystine to L-cysteine is generally more accepted as an effective method of generating the amino acid. This is generally done chemically *via* catalytic hydrogenation using tin in hydrochloric acid, following *Equation 1-1*[5].

Equation 1-1

$$RSSR + 2M - H_{(ads)} \longrightarrow 2RSH + 2M$$

This process works quite well, however, as it is generally carried out in hydrochloric acid on tin, large amounts of hazardous waste is created in an industrial setting. Electroreduction of cystine is therefore the more popular route for large scale production of high purity L-cysteine. This process (*Equation 1-2*[5]) normally results in the creation of the hydrochloride salt, which can then be converted to the free base *via Equation 1-2*

$$RSSR + 2H^+ + 2e^- \longrightarrow 2RSH$$

an electrodialysis step. The free base, however, is more susceptible to oxidation back to L-cystine, and therefore the produced L-cysteine is often transported and sold as the acid salt, then converted to the free base on site when needed. The L-cystine required for this process is extracted from acid hydrolysates of keratins from hair, horn, hooves, feathers and wool[5].

1.3.3 Applications of Cysteine

As with all amino acids, only the L form of cysteine is found naturally, as such it is generally the L form which is attractive to industry. It has many uses in the food industry. It is used in the production of dough for bread and pasta to improve softness, making the dough easier to work and decreasing baking time. As well it is used in the production of seasonings which have a meat flavour and as an anti-oxidant in natural fruit juices[5].

Cysteine has also been shown to have a significant effect on skin and hair as it can break and reform the disulfide linkages integral to the structure of the proteins

which make up these materials. As a result it is used in the treatment of seborrhea, acne, dandruff and in less destructive “perms” for women’s hair[5].

The pharmaceutical industry has also taken advantage of L-cysteine. There are several drugs produced from L-cysteine which are utilized to break down mucus in patients with bronchitis and nasal catarrh; other derivatives are used to combat hepatitis, respiratory disease, and skin disorders[5].

Cysteine monolayers adsorbed on gold have also found use as detectors for Cu(II) in water samples[6]. Multi-dentate ligands are also commonly used in chemosensors, however cysteine has the strong advantage of avoiding complexation of interferants from the sample matrix, making it more attractive for this type of sensor[6]. L-cysteine adsorbed on gold has also been used to look at plasma protein and antisera interactions[1]. Gold slides were modified with either L-cysteine or 3-mercaptopropionic acid (MPA). The slides were then incubated in plasma then antisera serially. It was determined which antibodies were bound to the different slides, providing insight into how the antisera interacts with plasma in blood[1].

There have also been several investigations performed on cysteine as an environmentally safe corrosion inhibitor for copper[3,7]. It is well established that many nitrogen and sulfur containing organic compounds provide an inhibitory effect to copper corrosion, however the most commonly used of these compounds are nitrogen containing aromatic chemicals, which have been shown to have carcinogenic and other side effects[8]. Cysteine, however, is well suited to adsorption onto a copper

surface *via* the thiol group, and is biocompatible. In a study by Da Quan *et al.* it was discovered that cysteine was a more efficient corrosion inhibitor of copper in hydrochloric acid than benzotriazole, the most commonly used inhibitor used in the protection of copper[9]. Ismail's study in this area found that cysteine provided corrosion inhibition efficiency of approximately 84% for copper in neutral and acidic chloride solutions, as a result of adsorption of cysteine at the active corrosion sites of the metal[7].

1.4 Electrochemistry of Cysteine on Ag

Cysteine strongly adsorbs onto silver (Ag) *via* a Ag-sulfide linkage[10]. The adsorption is so strong that no desorption peak is observed, even at very negative potentials. The cysteine will remain adsorbed to the Ag surface until hydrogen evolution occurs and the metal itself is damaged[11].

Paik *et al.* proposed mechanisms for the adsorption of thiols and dialkyl disulfides onto gold and Ag surfaces[12]. From electrochemical and quartz crystal microgravimetric measurements it was observed that thiol molecules adsorb onto the Ag surface through a process resulting in an anodic current whereas dialkyl disulfides adsorption onto Ag produces a cathodic current. The adsorption mechanisms for a thiol and for a dialkyl disulfide are shown, in *Equation 1-3* and *Equation 1-4*.

Equation 1-3

$$RSH + Ag \longrightarrow RS - Ag + H^{+} + e^{-}(Ag)$$

Equation 1-4

$$RSSR + Ag + e^{-}(Ag) \longrightarrow RS - Ag + RS^{-}$$

It is of note that although *Equation 1-4* shows a net one electron transfer, the full process involves the two electron reduction of the dialkyl disulfide, while a one electron oxidation of the Ag occurs simultaneously. The RS^{-} produced from this reaction has two main pathways which it will then follow. One is adsorption onto the Ag surface in a reaction very similar to that of the thiol (*Equation 1-5*).

Equation 1-5

$$RS^{-} + Ag \longrightarrow RS - Ag + e^{-}(Ag)$$

The unbound RS^{-} can also diffuse away from the surface and either protonate to the thiol or oxidize back to the dialkyl disulfide[12].

As was discussed in Section 1.1 , cysteine is readily oxidized to the dimer cystine in a reversible reaction. Watanabe and Maeda observed that L-cystine could be reduced to L-cysteine in a quasi-reversible redox cycle when L-cystine was adsorbed on to a polycrystalline Ag electrode (*Equation 1-6*)[10].

Equation 1-6

$$RSSR_{(ads)} + 2e^{-} \overrightarrow{\longleftarrow} 2RS^{-}_{(ads)}$$

Conversely, when L-cysteine was adsorbed onto the Ag electrode, oxidation to cystine was not observed. This was an interesting result which was resolved using surface enhanced Raman scattering (SERS) measurements. SERS data indicated that L-cystine was adsorbed onto the Ag surface in a configuration where the disulfide

bond was tilted away from the surface to a certain degree. When the L-cystine is reduced to two L-cysteine molecules, the strong Ag-S bond ensures that both new molecules will be adsorbed onto neighbouring Ag atoms. The orientation of the L-cysteine molecules upon adsorption to the Ag surface is similar to their orientation when formed into L-cystine. Therefore when an anodic current applied to the electrode the L-cysteine molecules are oxidized to re-form L-cystine[10].

This pathway is not available when L-cysteine is adsorbed directly onto a Ag electrode. In this situation the L-cysteine molecules will adsorb onto the Ag in a configuration which will minimize steric hindrance between adjacent molecules. In this configuration it is not favourable for the L-cysteine molecules adsorbed on neighbouring Ag atoms. Due to the strong Ag-S bond preventing surface diffusion the L-cysteine cannot move into a position where the oxidation of L-cysteine to L-cystine is possible, thus L-cysteine remains in its monomeric form.

1.5 Second Harmonic Generation

Optical second harmonic generation (SHG) is a second order nonlinear optical process which can be simply described as "the nonlinear conversion of two photons of frequency ω to a single photon of frequency 2ω"[13]. In general terms the polarization of radiation produced from a material can be expressed as a sum of all the components (*Equation 1-7*[13]).

Equation 1-7

$$P = \chi^{(1)}E^1 + \chi^{(2)}E^2 + \chi^{(3)}E^3 + \ldots$$

P is the polarization induced by excitation with a radiation source, where $\chi^{(n)}$ is the *n*th order susceptibility constant and E is the electric field. The *n*=1 term describes normal absorptive and reflective processes. The *n*=2 term therefore describes second harmonic generation and will therefore be the main focus of this discussion[13].

There are several different sources of second harmonic radiation from metals; however the simplest description of this effect is explained using the electric dipole approximation. The polarization of the SH radiation alone can be expressed simply as shown below[14]

Equation 1-8

$$P^{(2)}(2\omega) = \chi^{(2)}E^2(\omega)$$

E(ω) is the amplitude of the electric field vector for the incident radiation, therefore $P^{(2)}(2\omega)$ will vary as a function of $\chi^{(2)}$. $\chi^{(2)}$ is a third order tensor with 27 different elements. These terms have the notations of χ_{XYZ} where X, Y and Z are Cartesian coordinates with Z being normal to the surface and X and Y being in the plane of the surface. Symmetry in a material will decrease the number of nonzero and independent elements which contribute to $\chi^{(2)}$. $\chi^{(2)}$ can be modeled by *Equation 1-9*[14].

Equation 1-9

$$\chi^{(2)} = -\zeta \frac{Ne^3}{2m^2} \frac{1}{(\omega_0^2 - \omega^2)^2(\omega_0^2 - 4\omega^2)}$$

There are three variables in this expression which define the magnitude of $\chi^{(2)}$ *N*, ω_0 and ζ. *N* is the number of electrons in the system of interest, implying that for molecules adsorbed on a surface $\chi^{(2)}$ should increase with surface concentration[14]. For metals, *N* is related to the density of free electrons at the metal surface. In this instance *N* (and $\chi^{(2)}$) can therefore be considered to be inversely proportional to the work function of the metal.

ω_0 is the plasma frequency of the material being probed and ω is the frequency of the incident radiation. As can be seen from *Equation 1-9* when $\omega \to \omega_0 \text{ or } \frac{1}{2}\omega_0$ a zero factor is created in the denominator, increasing $\chi^{(2)}$ and the probability of SHG to occur. This is the source of the resonance enhancement sometimes observed in SH studies[14]. An energy level diagram showing the mechanisms for resonance enhanced SHG is shown in Figure 1.3.

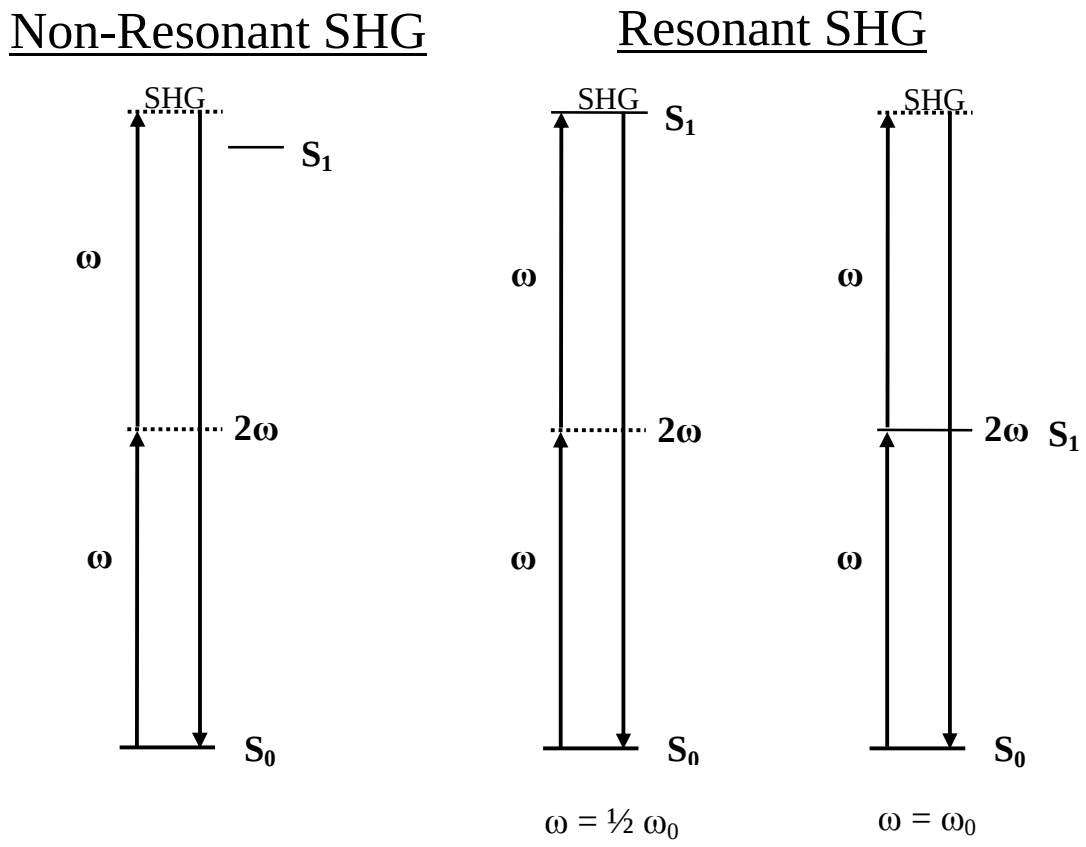

Figure 1.3 - Jablonski diagram depicting the resonance enhancement for SHG.

1.5.1 Surface Selectivity of SHG

One of the most important characteristics of SHG under the electric dipole approximation is that the medium being investigated must be noncentrosymmetric *ie.* the medium must have no inversion symmetry. This phenomenon is based on the concept that a reversal of an axis in the plane of the surface, as would occur in a medium with inversion symmetry, should result in a change in sign of the polarization. However, the reversal of that axis also implies a change in sign of the

electric field. From *Equation 1-8* it is noticed that $E(\omega)$ is squared, thus leaving $P^{(2)}$ unchanged. The only way both of these requirements can be fulfilled is if $\chi^{(2)}=0$, resulting in no SH signal being generated[15]. In *Equation 1-9* ζ is the anharmonicity constant, the realization of the symmetry requirement of the electric dipole approximation.

The symmetry requirement preventing SHG from occurring in a centrosymmetric medium is widely exploited for the study of interfaces. Many media, such as gases, liquids and face centered cubic crystals are centrosymmetric in the bulk[16]. At an interface however, the symmetry of two bulk centrosymmetric materials will be broken due to the inherently different forces acting upon the molecules or atoms at the interface. This asymmetry is only observed for the top few layers of the medium, making this technique extremely sensitive to surface processes[14].

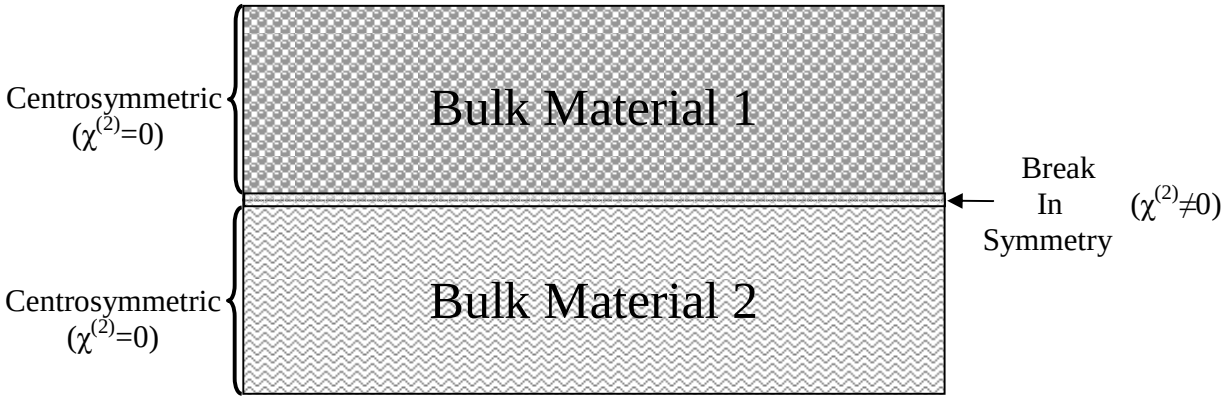

Figure 1.4 - Schematic of the source of surface selectivity in SHG experiments.

1.5.2 SHG from Interfaces

Under the dipole approximation (*Equation 1-9*) SHG is forbidden in centrosymmetric media such as the bulk of a face centered cubic crystal, however higher order sources of polarization such as the electric quadrupole and magnetic dipole terms can still occur[16,17]. *Equation 1-10* shows other contributions (beyond the dipole approximation) from both the surface and the bulk.

Equation 1-10

$$P_{s,eff}^{(2)} = \alpha[E(\omega)\bullet\nabla E(\omega)] + \beta E(\omega)[\nabla\bullet E(\omega)] + \left(\frac{2i\omega}{c}\right)\gamma[E(\omega)\times B(\omega)] + \chi_s^{(2)}\delta(z):E(\omega)E(\omega)$$

In this equation $B(\omega)$ is the magnetic field of the incident laser, $\chi_s^{(2)}$ is the surface nonlinear susceptibility and $\delta(z)$ is a delta function at $z=0^+$ [17]. The first two terms can be attributed to the electric quadrupole, the third to the magnetic dipole, and the last term to the electric dipole contribution[17]. When the excitation source is plane polarized however, the first term disappears and in a homogeneous medium the second term vanishes as well. This allows for the electric quadrupole terms to be neglected. In the third term the induced polarization is along the direction of propagation of the exciting light, thus only the polarization is able to radiate from the surface[17]. From the above relationship the intensity of the reflected second harmonic signal follows *Equation 1-11*.

Equation 1-11

$$I^{2\omega} = \frac{32\pi^3\omega^2\sec^2\theta_{2\omega}}{c^3\varepsilon_1(\omega)\varepsilon_1^{1/2}(2\omega)}\left|e(2\omega)\bullet\chi_{s,eff}^{(2)}:e(\omega)e(\omega)\right|^2 I^2(\omega)$$

where $\theta_{2\omega}$ is the angle of SH light with respect to the surface normal, $I(\omega)$ is the intensity of the excitation source, and $e(2\omega)$ is the polarization at the SH frequency. The corresponding Fresnel coefficients are included into each tensor element. It should also be noted that $\chi^{(2)}_{s,eff}$, the effective surface nonlinear susceptibility factor is composed of both $\chi^{(2)}_{s}$ as well as the bulk magnetic dipole contribution[17].

1.5.3 SHG from Metals

The characteristic properties of metals originate with the band structure of the electrons. The atomic orbitals in metals are so close together that the valence electrons of the metal atoms are delocalized across the entire surface, allowing for the movement of the electrons throughout the entire crystal structure. This phenomenon can be thought of as a gas of free electrons. Light incident on a metal surface will result in an oscillating polarization with both the fundamental and harmonic frequencies of the incident light apparent in this polarization[15]. The nonlinear polarizability of the electrons at a metal surface are generally quite high and as such dominate the SHG signal collected from metal surfaces[14]. For this reason adsorption processes on metal surfaces are usually studied indirectly in SHG experiments. As opposed to directly measuring the SHG from the adsorbate, the change in SHG from the metal surface is monitored. This change is most commonly as a result of a modification of the surface electronic states of the metal upon adsorption[14]. As mentioned previously above, the dipole contribution to SHG is proportional to N, the free electron density of the surface. This means that for systems where electronic

resonance is not a factor, adsorption of molecules onto the metal surface which increase the free electron surface density will also increase the surface SHG observed. Conversely, adsorption of molecules onto the metal surface which decrease the free electron surface density will decrease the surface SHG observed.

1.5.4 Second Harmonic Generation from a Potential Controlled Surface

Electric field induced second harmonic generation or EFISH is a phenomenon where an applied electric field induces a second harmonic response from a bulk centrosymmetric medium. This process can occur through either molecular realignment or the polarization of bonds in the sample[14]. EFISH can be described as adding another nonlinear polarization term ($P_E^{(2)}(2\omega)$) to the effective polarization of the SH light generated.

Equation 1-12

$$P_E^{(2)}(2\omega) = \chi^{(3)} : E_{DC} E(\omega) E(\omega)$$

As can be seem from *Equation 1-12*, $P_E^{(2)}(2\omega)$ is a third order nonlinear optical process which results in a frequency doubling. When combined with *Equation 1-8* an effective nonlinear susceptibility dependent on the cell potential, Φ, results[16].

Equation 1-13

$$\begin{aligned} P_{Eff}^{(2)}(2\omega) &= \chi^{(2)} : E(\omega) E(\omega) + \chi^{(3)} : E_{DC} E(\omega) E(\omega) \\ &= \chi_{eff}^{2}(\Phi) : E(\omega) E(\omega) \end{aligned}$$

It is expected that the component of $\chi^{(2)}_{eff}(\Phi)$ normal to the surface will vary linearly with the electric field applied across the interface, thus resulting in the parabolic behaviour of the SH signal as a function of potential, for systems where the normal

component of the nonlinear susceptibility dominates[16]. Separating the potential dependent parts from the independent ones yields *Equation 1-14* where $P_E^{(2)}(2\omega)$ *and* $P^{(2)}(2\omega)$ are the third and second order polarizations, *d* is the thickness of the electric double layer and δ is a factor to correct for the fact that the entire potential drop does not occur at the part of the interface that produces SH. $\Delta\Phi$ is the potential difference between the applied potential, Φ and the potential of zero charge, Φ_{pzc}. If we then define *a* as $e^{2\omega} \bullet P_E^{(2)}(2\omega)\delta d^{-1}$ and *b* as $e^{2\omega} \bullet P^{(2)}(2\omega)$, the parabolic relationship shown in *Equation 1-15* results.

Equation 1-14

$$P_{eff}^{(2)}(2\omega) = P_E^{(2)}(2\omega)\delta d^{-1}\Delta\Phi + P^{(2)}(2\omega)$$

Equation 1-15

$$I^{SHG} \propto | a(\Phi - \Phi_{pzc}) + b |^2$$

From *Equation 1-15* it is expected that the potential dependence of SHG generated from an electrode surface will be parabolic, with a minimum at the pzc. Experiments performed by Guyot-Sionnest and Tadjeddine on Ag(111) and Au(111) confirmed that this model was valid when the excitation source was not within the interband transition regime of the metal[18]. When the excitation source is in the interband transition regime of the metal it was found that the EFISH contribution to the SH signal was not as important and had little effect on the total SHG[18].

1.5.5 Study of Surface Symmetry *via* Rotational Anisotropy

As mentioned above, $\chi^{(2)}$ is composed of 27 tensor elements, denoted as χ_{XYZ}. The tensor elements which will contribute to $\chi^{(2)}$ from a surface are dependent on the average surface symmetry. This property allows for surface symmetry measurements to be performed *via* SHG measurements[14]. These measurements are performed using a setup shown schematically in Figure 1.5. In this schematic, the angle of incidence of the excitation laser and the collection of the SHG are fixed, as are the input and output polarizations. The sample is rotated about an azimuthal axis, generally corresponding to a crystallographic axis of the sample. Rotational anisotropy patterns are then obtained with various input and output polarizations, to study the different contributing $\chi^{(2)}$ tensor elements[14]. A clear example of the ability of these measurements to provide information regarding surface symmetry was performed by

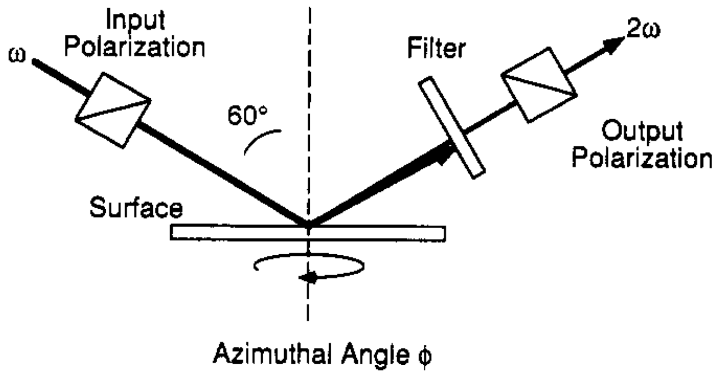

Figure 1.5 - Experimental set-up for SHG rotational anisotropy measurements. Reprinted with permission from Corn, R. M.; Higgins, D. A. *Chemical Reviews* **1994**, *94*, 107. Copyright 1994 American Chemical Society.

Corn *et al.*[14] In their study of iodine adsorbed on Pt. single crystal electrodes they were able to observe the three- and two-fold symmetry of the surface for a (111) and (110) surface. This correctly identified that the surface symmetry of the single crystal electrodes were C_{3v} and C_{2v} respectively[14].

1.6 Raman Scattering

Raman scattering was first discovered in 1928 by Raman and Krishnan[19]. They discovered that inelastic scattering of light occurred when a sufficiently powerful light source was used to illuminate a liquid or gaseous sample. Raman spectroscopy has known great success since then, and has become an integral tool used in the characterization of chemical systems. There have been several books and review articles written on this topic which cover the theory and application of Raman scattering in detail[20-26]. Only the fundamentals of these topics will be addressed.

Light scattered by molecules can have either the same, higher or lower energy as the incident light. The majority of light interacting with molecules does not change energy when scattered and is known as Rayleigh scattering. Raman scattering occurs when there is a transfer of energy between the incident radiation and the molecular scatterer. An example of the energy distribution of scattered radiation is shown in Figure 1.6. As can be seen from Figure 1.6 Raman scattering resulting in a loss of energy (Stokes shifted) is stronger than that resulting in a gain of energy (anti-Stokes shifted). The reason for this can be deduced from the Jablonski diagram shown in

Figure 1.7. The diagram shows that for an anti-Stokes Raman shift to occur the molecule being studied must be at a vibronically excited state before interacting with the incident light. The probability of this occurring follows a Boltzmann distribution therefore requiring elevated temperatures to provide a strong anti-Stokes Raman signal.

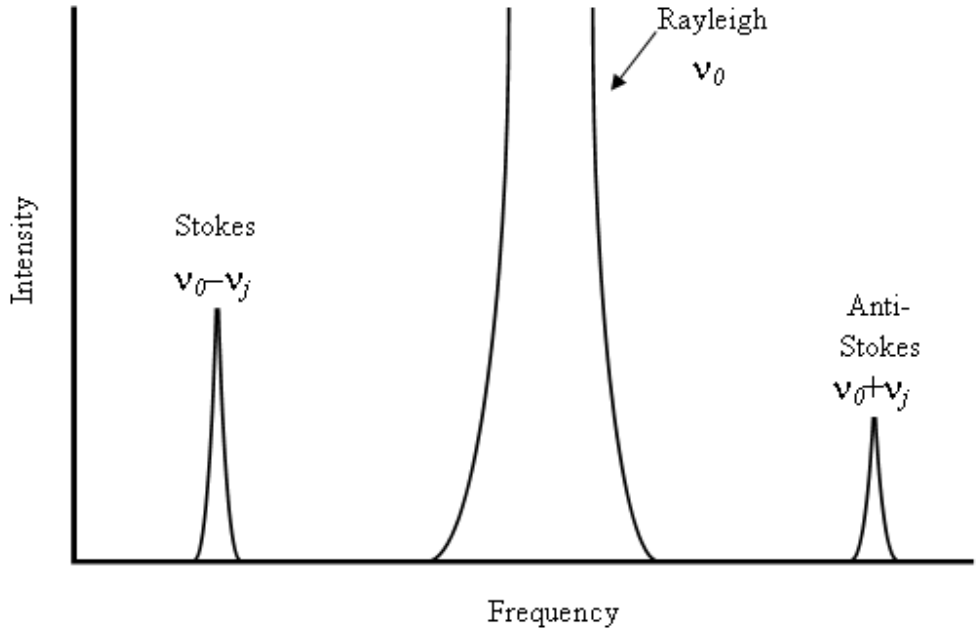

Figure 1.6 - Energy distribution of scattered radiation.

Another consequence of the Boltzmann dependence is that the anti-Stokes signal will decrease as the frequency shift increases. For these reasons only the Stokes shifted Raman data is usually collected, and is denoted as a positive shift by convention.

Figure 1.7 shows the energy level diagrams of the common vibrational spectroscopy techniques. Upon examination of that figure, there are several important

features which should be noted. The most important characteristic of Figure 1.7 is the energy of the vibrational mode of the molecule ΔE. It is evident that the ΔE for the Stokes and anti-Stokes processes have the same magnitude but opposite sign, thus collection of only the Stokes shifted data does not result in the loss of any vibrational bands. Similarly it is evident that ΔE for Raman and infrared (IR) are the same. It is for this reason that these two methods are considered to be complementary. The vibrational mode of a molecule will result in a Raman band at the same frequency as in an IR spectrum. These two methods do not result in identical spectra however, due to the different selection rules for IR and Raman spectroscopy. In IR spectroscopy the selection rules dictate that a vibration will only be IR active if a change in the dipole moment of the molecule occurs as a result of the vibration of the molecule. However, in Raman spectroscopy the selection rules allow for a vibrational mode to be observable only when the vibration results in a change in the polarizability of the molecule. Thus, although some bands may exist in both Raman and IR spectra, they will generally have a different strength. In addition there will be some vibrational modes which are either exclusively Raman or IR active, thereby allowing for a more complete vibrational profile to be generated by combining the data from both methods.

Also of note in Figure 1.7 is that for Raman processes the molecule is excited to a virtual state. Excitation to a real state will result in a resonance enhancement of the Raman signal, further discussed in section 1.6.2.

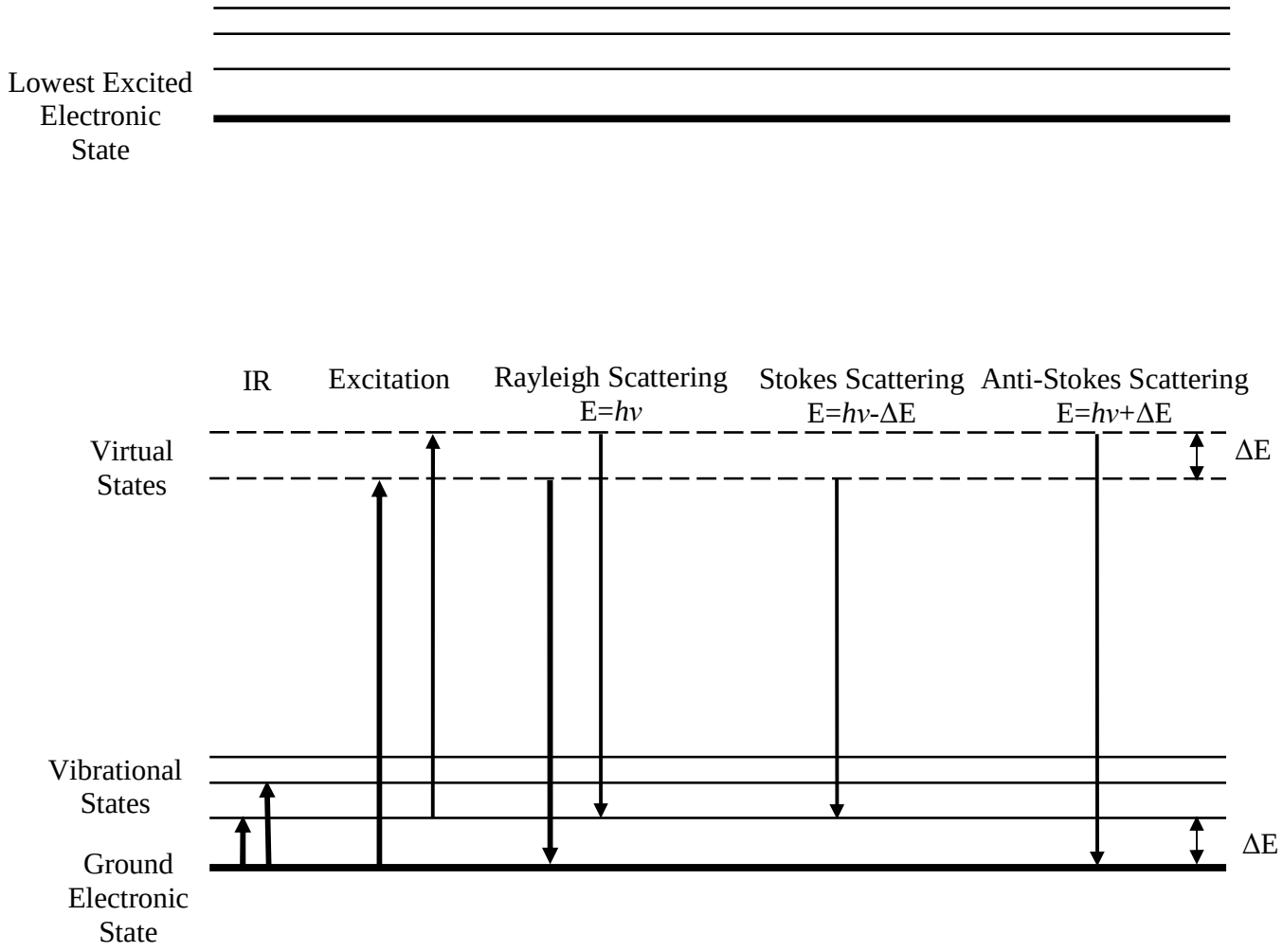

Figure 1.7 - Jablonski diagram showing IR absorption, Rayleigh scattering and Raman scattering

1.6.1 Classical Description of Raman Scattering

The classical explanation of Raman scattering[21,27] relies on the idea that the oscillating electric field of the incident light interacts with the molecular electronic cloud creating an induced dipole. This dipole then radiates light which may or may

not have exchanged energy with the internal vibrational modes of the molecule. The induced polarization (P) is related to the polarizability of the bond (α) and the incident electric field (E) in *Equation 1-16*.

Equation 1-16

$$P = \alpha E$$

A useful description of light scattering from a molecule starts with the definition of E, where ν_0 is the frequency of the incident light.

Equation 1-17

$$E = E_0 \cos 2\pi \nu_0 t$$

Molecular vibrations can be described as constituting of *3N-6* (for a non-linear molecule with N atoms) normal modes, Q_j. Q_j is related to ν_j, the harmonic frequency of the jth mode, as in *Equation 1-18*.

Equation 1-18

$$Q_j = Q_j^0 \cos 2\pi \nu_j t$$

The nuclear displacements caused by the vibration of a molecule will modify the polarizability of the electrons in the molecule, which can be described by a Taylor series in *Equation 1-19* (of which only the two most important contributions are shown).

Equation 1-19

$$\alpha = \alpha_0 + \left(\frac{\delta \alpha}{\delta Q_j} \right)_0 Q_j + \ldots$$

Substituting *Equation 1-18* into *Equation 1-19* and then substituting this result and *Equation 1-17* into *Equation 1-16*, a more detailed description of the polarization of the *j*th band results.

$$P_j = \alpha_0 E_0 \cos(2\pi\nu_0 t) + E_0 Q_j^0 \left(\frac{\delta\alpha}{\delta Q_j}\right)_0 \cos(2\pi\nu_0 t)\cos(2\pi\nu_j t)$$

Employing the trigonometric identity $\cos(x)\cos(y) = \frac{1}{2}[\cos(x+y) + \cos(x-y)]$ result in

Equation 1-20

$$P_j = \alpha_0 E_0 \cos(2\pi\nu_0 t) + \frac{1}{2} E_0 Q_j^0 \left(\frac{\delta\alpha}{\delta Q_j}\right)_0 \cos[2\pi(\nu_0 + \nu_j)t] + \frac{1}{2} E_0 Q_j^0 \left(\frac{\delta\alpha}{\delta Q_j}\right)_0 \cos[2\pi(\nu_0 - \nu_j)t]$$

This relationship is very useful as it depicts most of the characteristics of scattered light. The first term predicts Rayleigh scattering at ν_0 while the second and third terms describe Raman anti-Stokes and Stokes scattering at $\nu_0+\nu_j$ and $\nu_0-\nu_j$ respectively. Most importantly, this expression illustrates the result of the selection rules for Raman scattering; that a vibrational mode must result in a change in the polarizability with the vibration to be Raman active. It is obvious in *Equation 1-20* that if there is no change in the polarizability during a particular vibrational mode, $(\partial\alpha/\partial Q_j)_0 = 0$, then the mode will not contribute to a Raman spectrum.

1.6.2 Resonance Raman Scattering

One important aspect of Raman scattering which cannot be accounted for by the classical model described in Section 1.6.1, is the resonance enhancement observed

when the molecule is excited to a real state instead of a virtual state. Typically only 1 in 10^{10} photons are Raman scattered, thus a significant effect which can increase a Raman signal by 10^2-10^6 times is very important to understand. To obtain the proof of this phenomenon a more complex quantum mechanical approach is required. A more detailed description of the quantum mechanical model for Raman scattering can be found elsewhere[24,27]. Provided without derivation is the result of the calculation of the transition dipole moment between two vibrational states *via* a virtual state required to quantum mechanically model Raman scattering.

Equation 1-21

$$\left(\alpha_{\rho\sigma}\right)_{fi} = \sum_{v \neq f,i} \left(\frac{\left\langle \psi_f \mid \hat{P}_\rho \mid \psi_v \right\rangle \left\langle \psi_v \mid \hat{P}_\sigma \mid \psi_i \right\rangle}{E_{vi} - E_0 - i\Gamma_v} + \frac{\left\langle \psi_f \mid \hat{P}_\sigma \mid \psi_v \right\rangle \left\langle \psi_v \mid \hat{P}_\rho \mid \psi_i \right\rangle}{E_{vf} + E_0 + i\Gamma_v} \right)$$

Equation 1-21 shows the polarizability of the molecule $(\alpha_{\rho\sigma})_{fi}$ as the sum of the components of the polarizability between the initial and final states. The wavefunctions of the final, virtual and initial states are ψ_f, ψ_v, and ψ_i respectively and $\hat{P}$ is the electric dipole operator. E_{vi} is the energy difference between the virtual and initial state, E_{vf} is the energy between the virtual and final state and E_0 is the energy of the incident light. The final term, $-i\Gamma_v$ is a damping term, employed to ensure that division by zero does not occur under resonance conditions.

It is clear that when $E_{vi}=E_0$ the denominator of the first term of *Equation 1-21* will be dependent only on $-i\Gamma_v$. If $E_{vi}=E_0$ results in excitation to a real electronic state, the lifetime of the state will be greatly increased compared to that of a virtual state. Since $-i\Gamma_v$ is inversely proportional to lifetime, this scenario will result in a very large

first term. This is the source of the resonance enhancement observed for certain systems being studied by Raman spectroscopy. This is a useful tool in bioimaging, as the need for biolabels is eliminated due to the specificity of resonance Raman for a particular chromophore.

1.7 Surface Enhanced Raman Scattering

The phenomenon of surface enhanced Raman scattering (SERS) was first observed in 1974 by Fleischmann *et al.* for pyridine adsorbed on a rough silver surface[28]. However the enhancement was incorrectly solely attributed to a larger surface area of the rough surface, resulting in more scatterers being present. In 1977 it was independently recognized by Jeanmaire and Van Duyne[29] and Albrecht and Creighton[30] that increased surface area alone could not account for the large Raman enhancement observed and that the adsorption of the analyte molecules onto the metal surface must play a part in the phenomenon.

SERS typically exhibits an enhancement of four to six orders of magnitude relative to a normal Raman signal. The discovery of SERS created a greatly rejuvenated interest in Raman spectroscopy as it was now possible to address one of the largest issues regarding Raman spectroscopy, the low efficiency of the process. SERS is now a well established technique with many applications in analytical and biochemical settings[31].

The actual mechanisms responsible were in dispute for some time. Originally Jeanmaire and Van Duyne proposed a mechanism whereby an electric field enhancement at the surface was responsible for the phenomenon[29]. Albrecht and Creighton however were of the opinion that the enhancement was due to a resonance Raman effect observed due to the broadening of the electronic molecular orbitals of the molecule upon adsorption onto the surface[30]. These two theories developed into the main theory accepted to be responsible for the enhancement now. They are the electromagnetic (EM), and the chemical or charge transfer (CT) mechanisms. It is now widely accepted that the EM mechanism is largely dominant in SERS, generally contributing a 10^4-10^5 enhancement, with the CT mechanism being responsible for the remaining 10-10^2 enhancement[27].

1.7.1 The Electromagnetic Enhancement Mechanism of SERS

The electromagnetic enhancement (EM) mechanism of SERS shows the enhancement to be related almost entirely to the properties of the substrate. The only aspect of the adsorbate that comes into play in the EM mechanism is distance from the surface. Empirical results indicate that the enhancement is evident only for sub-wavelength scale features on specific metals (notably Ag, Au and Cu).

The principle underlying the EM mechanism is that the local electromagnetic field is increased in the vicinity of the studied analyte. This is accomplished through the excitation of surface plasmons. Surface plasmons are oscillations of the free electrons of a metal surface. On a smooth surface the surface plasmons are confined

and cannot couple with the incident photon due to a momentum mismatch[32,33]. A rough or nanostructured surface however will provide additional momentum to the incident photon, allowing for coupling between the surface plasmon and the photon. This process results in the redistribution of the energy of the electromagnetic field into so-called “hot spots”. This implies that analyte molecules which are adsorbed at these hot spots will be favoured since they will have an enhanced Raman signal. This mechanism is depicted in Figure 1.8.

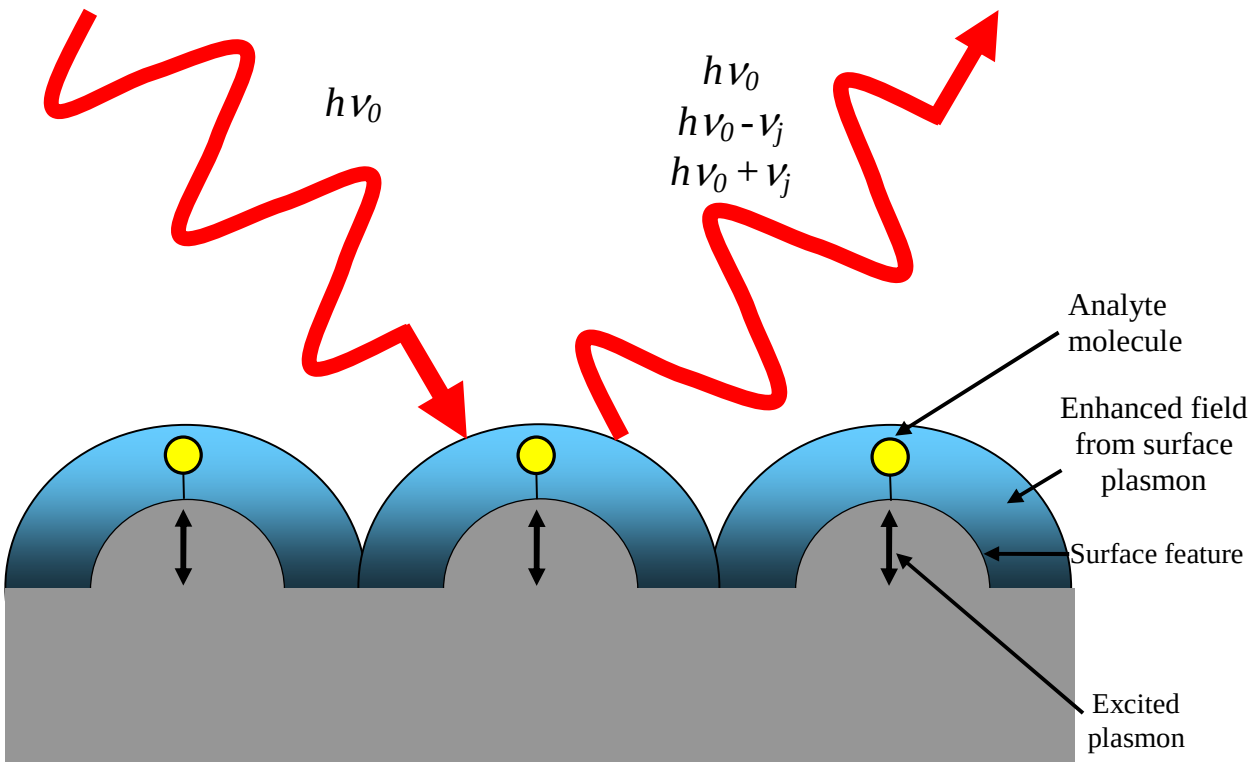

Figure 1.8 - Schematic showing the principle of the electromagnetic (EM) enhancement mechanism for SERS.

A simple and useful way to understand the properties of the EM enhancement mechanism is to approximate a SERS active substrate as a metal sphere smaller than the wavelength of excitation [34,35]. This approach provides us with several important trends when considering SERS. The first is that a smaller sphere has a stronger maximum enhancement than a bigger sphere. This increased enhancement comes at the price of a decreased range of exciting wavelengths across which it is effective. Kerker *et al.* showed that a 50 nm silver sphere will create an enhancement of 10^4 over several hundred nanometers in the visible range, whereas a 5 nm sphere of the same type generates an enhancement greater than 10^6, though only over a few tens of nanometers[34].

The small metal sphere model also provides a relationship between the optical dielectric constant and the local electromagnetic field (*Equation 1-22*)[36].

Equation 1-22

$$\frac{E_{sphere}}{E_{normal}} \propto \frac{\varepsilon_1(\omega) - \varepsilon_2(\omega)}{\varepsilon_1(\omega) + 2\varepsilon_2(\omega)}$$

$\varepsilon_2(\omega)$ is the optical dielectric constant of the surrounding medium and $\varepsilon_1(\omega)$ is the complex optical dielectric function of the metal defined in *Equation 1-23*.

Equation 1-23

$$\varepsilon_1(\omega) = \mathrm{Re}[\varepsilon_1(\omega)] + i\,\mathrm{Im}[\varepsilon_1(\omega)]$$

Examination of *Equation 1-22* and *Equation 1-23* reveals that a major enhancement will be observed if $\mathrm{Re}[\varepsilon_1(\omega)] = -2\varepsilon_2(\omega)$ and $\mathrm{Im}[\varepsilon_1(\omega)]$ is small. This relationship provides the basis for why SERS works for only a handful of metals using visible excitation. The optical dielectric constant of the metal will affect the frequency of the

surface plasmons, and therefore dictates which metals will provide a SERS enhancement in the visible range.

More complicated models take into account that more than one surface feature will contribute to the observed enhancement. Though this was accomplished using several different models all of the results indicated the same basic trend[37-39]. The interaction of the surface features significantly increases the EM enhancement with the maxima occurring at points of contact or voids between the features.

1.7.2 The Charge Transfer Enhancement Mechanism of SERS

In 2000 Xu *et al.* performed calculations looking at the effect of size, shape and spacing on the EM enhancement observed from coupled colloids[40]. This study concluded that the maximum enhancement factor which can be obtained from the EM mechanism is on the order of 10^{11}. However several different groups have reported enhancements as high as 10^{14} in independent studies[41-44]. This leads to a new question, how are these enormous enhancement factors attained? The answer is that a second enhancement mechanism, the charge-transfer (CT) mechanism, also contributes to the observed SERS enhancement.

The basis of the CT mechanism is that a complex is formed between the metal surface of the SERS substrate and the analyte molecule adsorbed on its surface (Figure 1.9). The HOMO and LUMO of the analyte molecule are close to the Fermi level of the metal substrate in such a complex, allowing for charge transfer between

the HOMO or LUMO and the Fermi level[36,45-48]. If the difference in energy between the HOMO or LUMO and Fermi level is close to the frequency of the incident light an enhancement is observed similar to the resonance Raman process described in Section 1.6.2. Potential applied to the metal surface will alter the Fermi level of the metal and thus the energy gap between the Fermi level and the frontier orbitals of the adsorbate indicating that the CT mechanism is potential dependent. The CT enhancement mechanism relies strongly on the chemical nature of the adsorbate and is therefore sometimes also referred to as the chemical mechanism.

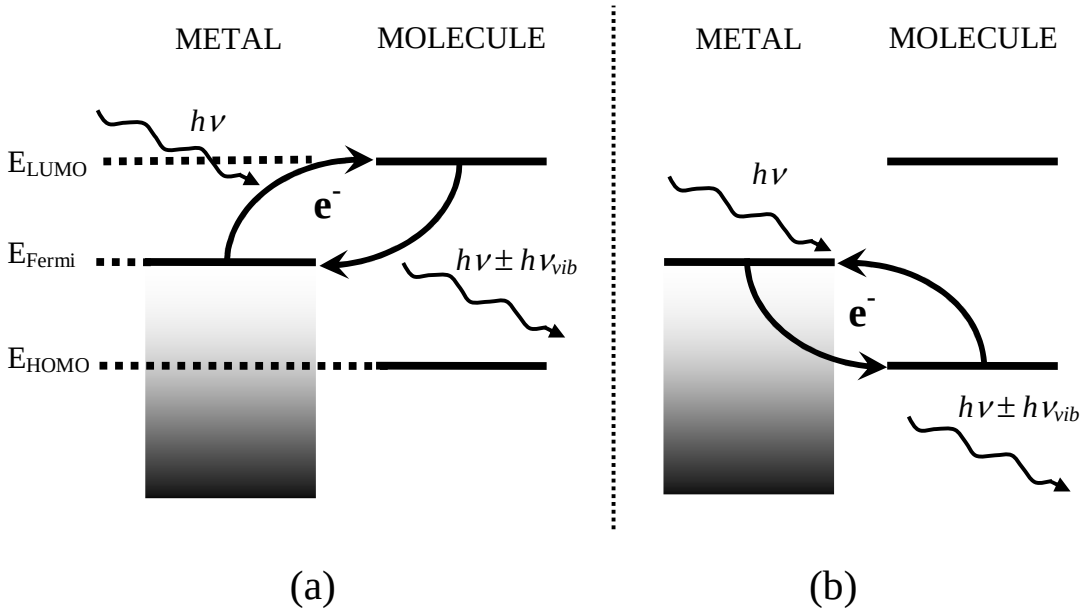

Figure 1.9 - Orbital diagram showing charge transfer enhancement mechanism for SERS. Electron transfer from the Fermi level of the metal to the LUMO of the adsorbed molecule and back (a), or from the HOMO of the adsorbed molecule to the Fermi level of the metal and back (b) can be in resonance with the incident photon $h\nu$. E_{Fermi} changes with applied potential.

Although the CT mechanism can contribute significantly to SERS spectra, it is considered only in specialized cases. The EM mechanism enjoys a much stronger enhancement and applies to many surface techniques, and therefore is often the only enhancement mechanism considered in SERS experiments, unless it is likely that a CT process will contribute in a meaningful way to the results.

1.8 *Ab initio* Calculations of Vibrational Modes

Ab initio calculations of the frequency of molecular vibrations are a useful tool in the assignment of band frequencies to specific molecular vibrations. A more complete description of these calculations can be found from several different sources[27,49,50].

All *ab initio* calculations rely on attempting to solve the Schrödinger equation for a molecular system. A significant drawback to *ab initio* calculations is the large time and computational power which would be required to perform the calculations without simplifications. There are therefore, many simplifications that have been developed with the goal of reducing these requirements.

One of the most prevalent ways of increasing the efficiency of the calculations is to simplify how the electrons in the system interact with each other. By allowing each electron to interact with the mean potential of all other electrons combined together as a single field, instead of in a pair-wise manner greatly simplifies the calculation. This method, known as the Hartree-Fock (HF) method, was first put

forward by Hartree[51] and later generalized by Fock[52]. A means for generating test wavefunctions is also needed to perform the calculation. The HF method allows for the wavefunctions to be approximated using linear combinations of atomic orbitals, though a basis set is required for a starting point for the atomic orbitals. Gaussian type orbitals (GTO)[53] are the most widely used approximation.

To accurately describe a wavefunction using the HF method requires 4 parameters per electron in the system. Unfortunately the Hamiltionian operator in the Schrödinger equation only deals with interactions between two particles at a time. This issue is overcome using density functional theory (DFT). According to DFT any system of electrons can be described by an electron density function. This changes the solution of the Schrödinger equation from many independent values to one function[54,55]. The DFT method does not; however, have procedures for generating an initial test function, therefore a HF calculation is normally used to produce this initial guess. As with most calculations of the properties of a molecule, DFT uses iteratively self-consistent fields (SCF). This allows for the progression of the calculation by using the solution of one iteration as the starting point for the next.

DFT calculations have found great use in many different areas of research, including vibrational spectroscopy. These calculations estimate the vibrational frequency of the different vibrational modes of a molecule. The calculated frequencies consequently serve as a good starting point for the assignment of the vibrational bands associated with experimental Raman spectra.

Chapter 2 - *In situ* Second Harmonic Generation Optical Rotatory Dispersion

This chapter presents the results of *in situ* SHG-ORD experiments performed to characterize the effect of a chiral adsorbate on the electronic structure of a metal. Cysteine in all its enantiomeric forms as well as 2-mercaptoethylamine (MEA) adsorbed on a polycrystalline Ag electrode were used to probe this relationship. An introduction highlighting the theory specific to these types of SHG experiments begins the chapter. Also included in the introduction is a review of the progress already made on the study of this system, as reported in the literature. The introduction is followed by a description of the materials and equipment used to perform the *in situ* SHG-ORD experiments. This is followed by the results of the experiments performed by our laboratory. The results were interpreted with the objective of determining whether the optical activity of the adsorbate would be evident in the electronic structure of the metal substrate. The final section summarizes the conclusions developed in the previous sections.

2.1 Introduction

Chiral molecules are extremely important in many modern fields of research. They are integral in the structure of all life forms, and are thus of great interest in many chemical, biological and medicinal applications[56]. This importance is due in great part to the chirality of amino acids and receptor sites which exhibit chiral

selectivity. Methodologies which can probe the properties of chiral surfaces are therefore extremely useful in furthering our understanding of these processes.

Traditionally, optical activity has been studied using various linear spectroscopies. The most common techniques used are linear optical rotatory dispersion (ORD) and circular dichroism (CD). CD takes advantage of the fact that the absorption of left and right circularly polarized light is different for different enantiomers. This method probes the imaginary part of the refractive index. There are two main constraints of doing CD experiments. Firstly, CD is a resonant technique, thus limiting the wavelength of light used as a probe. More importantly, however, is that the difference of the absorption between left and right circularly polarized light is small, typically being approximately 0.1% of the magnitude of the absorption[57].

ORD is a non-resonant process which relies on the difference between the real parts of the indices of refraction of left vs. right circularly polarized light on a sample. It is generally measured as the rotation of linearly polarized light as the light passes through the chiral medium. This effect is concentration dependent and, as with most linear spectroscopies, not surface sensitive.

To gain new insight into the optical activity of chiral surfaces, ORD and CD have been coupled with second harmonic generation, creating SHG-ORD and SHG-CD respectively. SHG-CD consists of comparing the SHG intensity of left and right hand circularly polarized fundamental beams. SHG-CD benefits from a stronger spectroscopic effect than its linear counterpart. This is due in large part to the

dominant role that the electric dipole plays in SHG experiments, overriding the comparatively weak magnetic and electric quadrupole terms responsible for the linear effect[57]. SHG-CD does still suffer from a reduced range of probe wavelengths which can be used. For this effect to be observed the molecules being studied must be in resonance with the exciting laser light, either at ω or 2ω. The financial cost for a tuneable laser system which would provide the power required for SHG is high, thus limiting the range of molecules which can be studied.

SHG-ORD experiments are conducted by exciting an SHG signal using a fundamental beam with fixed linear polarization, *p*. The rotation of the SHG signal is then determined and can be related to the chirality of the sample. Similarly to SHG-CD, SHG-ORD is surface sensitive and chiral selective, but additionally can be performed under off resonance conditions. Another great advantage of SHG-ORD is that the rotation angle of the generated light, ϕ, is dependent on the enantiomeric excess of the chiral molecule, but not the concentration of molecules[57]. This is useful because it means that very small quantities of a chiral material, such as a monolayer, will result in a measureable shift.

There are many examples of how SHG-ORD has been utilized to study the optical activity of molecules at various surfaces such as Langmuir-Blodgett films, the air/water interface, the air/quartz interface and the water/CCl_4 interface[57-59]. The optical activity observed in SHG-ORD experiments can be described by considering the nonzero, independent $\chi^{(2)}$ elements for an isotropic surface[57]. In this situation, the

27 elements of $\chi^{(2)}$ can be reduced to four nonzero independent terms, $\chi_1, \chi_2, \chi_3, and\ \chi_4$ shown below.

$\chi_1 = \chi_{zzz}$
$\chi_2 = \chi_{zxx} = \chi_{zyy}$
$\chi_3 = \chi_{xzx} = \chi_{yzy} = \chi_{xxz} = \chi_{yyz}$
and
$\chi_4 = \chi_{xyz} = -\chi_{yxz} = \chi_{xzy} = -\chi_{yzx}$

When the surface is isotropic and achiral there are mirror planes perpendicular to the surface, and thus χ_4 vanishes. When the surface is chiral the mirror planes perpendicular to the surface do not exist and thus all four tensor elements are required to describe the nonlinear behaviour of the surface. $\chi_1, \chi_2, and\ \chi_3$ are thus designated as the achiral elements of $\chi^{(2)}$,while χ_4 is known as the chiral element[57]. The rotation angle ϕ of the generated second harmonic signal is the amount by which the SHG signal is rotated with respect to any rotation caused by a racemic mixture of enantiomers. ϕ is defined by the *s* and *p* components of the electric field of the SHG signal.

Equation 2-1

$$\phi = \tan^{-1}\left(\frac{E_{2\omega}^{s}}{E_{2\omega}^{p}}\right)$$

Expansion of *Equation 2-1* and use of *p* polarized fundamental light to simplify the terms results in Equation 2-2[57].

Equation 2-2

$$\phi = \tan^{-1}\left[\frac{-\chi_4 \cos\theta}{\chi_1 \sin^2\theta + (\chi_2 - 2\chi_3)\cos^2\theta}\right]$$

Where θ is the angle of incidence of the fundamental beam[57]. ϕ is dependent on the chirality of the system, which in turn is communicated through the sign and magnitude of χ_4, the chiral tensor element. The sign of χ_4 reverses for opposite enantiomers, while the achiral terms remain unchanged, thus it is evident that the sign of ϕ will change when the handedness of the enantiomer being studied is switched[57]. This trend is clearly represented in Figure 2.1 where Byers *et al.* studied R- and S-2,2'-dihydroxy-1,1'binaphthyl, R- and S-BN, at the air water interface. The SHG-ORD data collected was fit to a cosine squared function, and the position of the maximum provided ϕ. In this example, ϕ of the racemic mixture was set as $\phi = 0°$. The R- and S- BN were shown to have $\phi = 17°$ and $\phi = -17°$ respectively[57].

Perhaps one of the more interesting applications of SHG-ORD is the characterization of molecules adsorbed at metal surfaces. Understanding this system has major implications for the study of the chiral properties of surface reactions such as in heterogeneous catalysis as well as the enantioselectivity of surfaces[57].

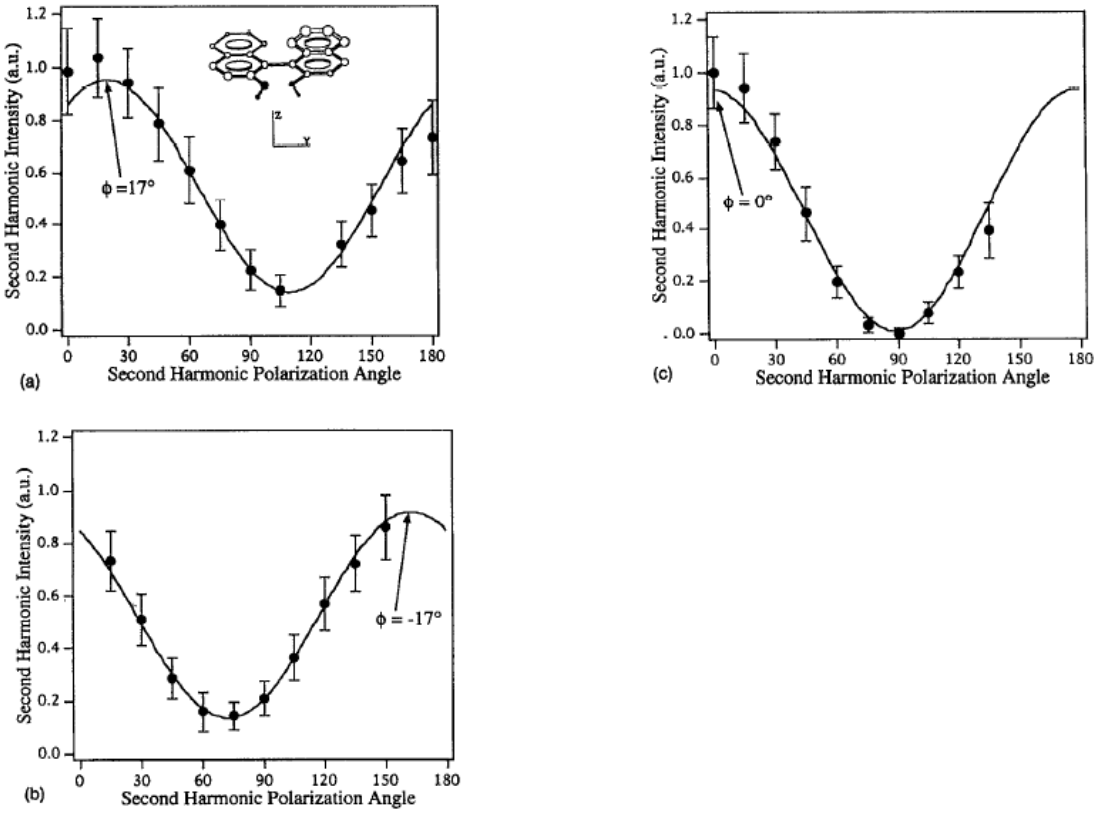

Figure 2.1 – Polarization analyzed SHG signal from air/water interface for saturated aqueous solutions. The samples are *R*-BN (a) *S*-BN (b) and a 50:50 racemic mixture of *R*- and *S*-BN (c) Reprinted with permission from [Byers, J. D.; Yee, H. I.; Hicks, J. M. *The Journal of Chemical Physics* **1994**, *101*, 6233.].Copyright [1994], American Institute of Physics.

The most notable studies conducted in this field have been carried out by Kadodwala *et al.*[60-62]. They conducted experiments where molecules were adsorbed on metal surfaces *ex situ*. As previously discussed (Section 1.5.3), SHG from metals is generated due to the large polarizability of the free and bound electrons found at the metal surface. This provides an extremely strong SHG signal from metal surfaces which will dominate the SHG signal which might be generated from any adsorbates

on the metal surface. Upon first inspection this could be seen as completely masking the signal from the analyte of interest. However it was suggested that chiral molecules adsorbed on the metal surface could imprint their chiral signature onto the electronic structure of the metal. SHG-ORD could then be used in the characterization of the optical activity of the metal instilled by the adsorbate[60,62].

In the experiments performed by Kadodwala *et al.*, an asymmetry was indeed observed in the SHG-ORD plots collected however, it was not in the form of a cosine squared function as predicted by Byers *et al*[57]. As seen in Figure 2.2 the asymmetry takes the form of a deformation of the plots, skewing the data to the right and left for R- and S-1-(1-naphthyl)ethylamine (NEA) respectively. The bare metal showed no deformation[62]. The expected fit could not be performed on this data, so to quantify the asymmetry I_{45}/I_{-45} and I_{-45}/I_{45} values were calculated. This is done by taking a ratio of the SHG intensity at +45º and -45º, where 0º is the maximum of the SHG-ORD plot. If chiral perturbation is present I_{45}/I_{-45} for one enantiomer will be equal to I_{-45}/I_{45} for the opposite enantiomer. Within the experimental error, the I_{45}/I_{-45} ratio for one enantiomer was equal to the I_{-45}/I_{45} ratio for the other. This phenomenon was therefore attributed to the optical activity of the NEA imprinting onto the electronic structure of the Cu(111) metal[62].

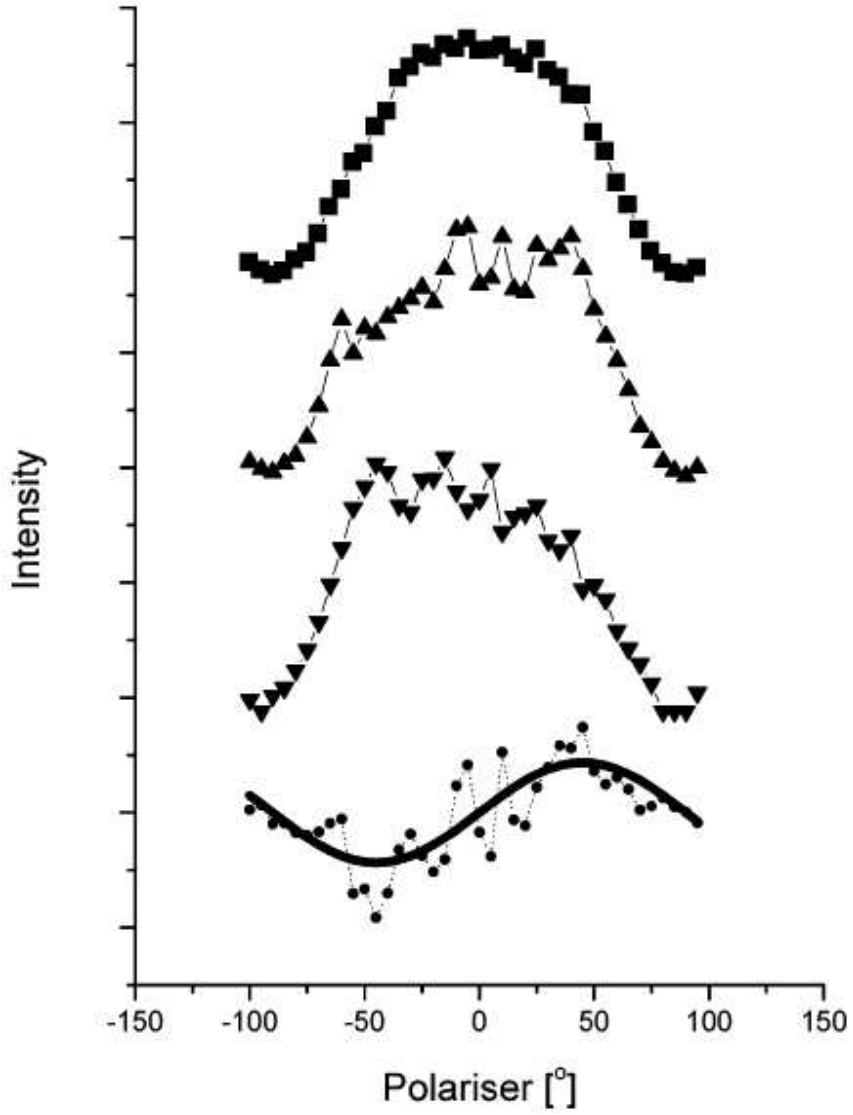

Figure 2.2 – SHG-ORD profiles for obtained after desorption of NEA layer (squares) and layers of R- (up-triangle) and S- (down-triangle) NEA are displayed. An R-S difference profile (circles) is also displayed along with the best-fit $\sin^2\Phi$ curve. The polarizer angle has been defined such that 0° is outgoing *p*-polarization. The data in the R and S profiles display a greater noise level than that collected for the postdesorption profile. Reprinted with permission from Mulligan, A.; Lane, I.; Rousseau, G. B. D.; Johnston, S. M.; Lennon, D.; Kadodwala, M. *Journal of Physical Chemistry B* **2006**, *110*, 1083. Copyright 2006 American Chemical Society

Although an effect was observed for NEA, not all chiral adsorbates were observed to instil chirality onto the electronic structure of the metal. The reason for this discrepancy was that adsorption geometry also contributes to the imprinting of optical activity onto the metal[62]. From this study it was believed that an adsorption geometry where a minimum of three chiral groups interact with the metal surface is required for the optical activity to be present in the electronic structure of the metal. This so called "chiral footprint" theory was further expanded when Kadodwala *et al.* studied cysteine adsorbed on gold slides[60]. A chiral signal was still observed, despite cysteine not interacting with the gold surface *via* three chiral groups. Further analysis revealed that the symmetry properties of the adsorbed molecular overlayers facilitate chiral perturbation in the electronic structure of the metal. In this way chiral adsorbates without an individual chiral footprint can still implant a chiral signature into the SHG signal observed from a metal substrate *via* the structure of the overlayers[62].

The SHG-ORD plots obtained for cysteine adsorbed on gold slides by Kadodwala *et al.* did not show the same skewed asymmetry of the NEA/Cu(111) system previously studied[60,62]. As can be seen from Figure 2.3, the plots presented trends more in keeping with those predicted by Byers *et a*[57]. SHG-ORD rotation angles (ϕ) were not presented by Kadodwala *et al.* The chirality was again measured by I_{45}/I_{-45} and I_{-45}/I_{45} values. These results demonstrated that a slight chiral perturbation was present in the SHG signal collected.

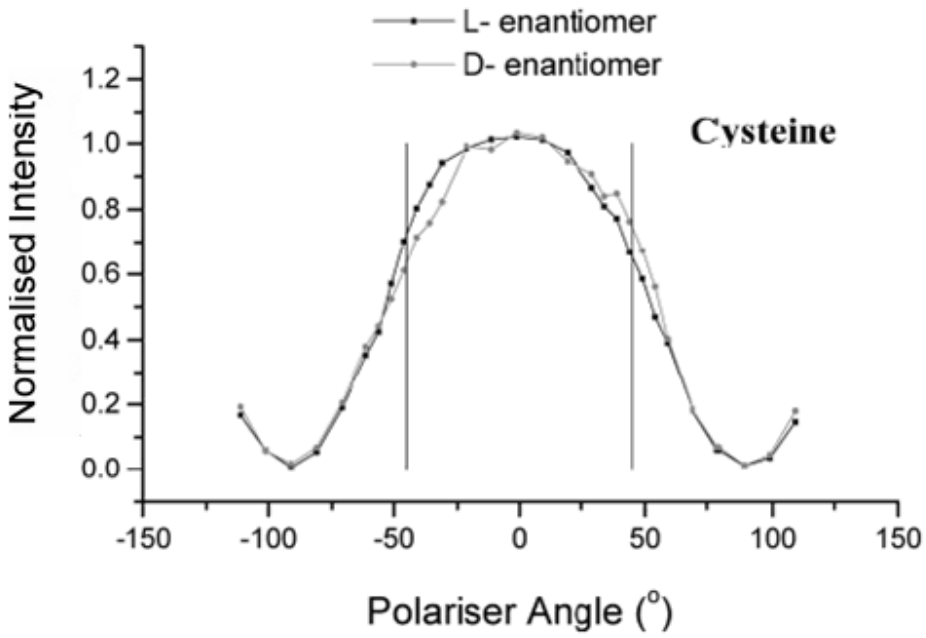

Figure 2.3 – SHG-ORD profiles for cysteine adsorbed on Au slides under acidic conditions. Angle is defined as being relative to out-going *p*-polarization. Solid lines inserted at ±45º. Adapted with permission from Bovet, N.; McMillan, N.; Gadegaard, N.; Kadodwala, M. *The Journal of Physical Chemistry B* **2007**, *111*, 10005.. Copyright 2007 American Chemical Society.

The studies conducted by Kadodwala *et al.* are useful as a demonstration that optical activity of a chiral adsorbate can be imprinted onto the electronic structure of a metal substrate and subsequently characterized *via* SHG-ORD experiments. There are still additional studies which could provide valuable results towards furthering the understanding of these processes though. One interesting prospect would be to perform SHG-ORD experiments *in situ* under electrochemical control. As the electronic structure of the metal is what is directly responsible for the SH signal generated, further control over this aspect of the experimental system could provide a

worthwhile new avenue of research. Along with this new direction, further studies would benefit from data collection over a more complete set of rotation angles of the output polarizer. This would allow for a better fit of the data, and for optical activity to be expressed as the more identifiable SHG-ORD rotation angle, ϕ.

2.2 Experimental

2.2.1 *In Situ* Second Harmonic Generation Optical Rotatory Dispersion (SHG-ORD) Instrumentation

In situ SHG-ORD experiments were performed using the experimental set-up represented schematically in Figure 1. An Innova 400 Ar^+ ion laser producing a 13.1 W beam was used to pump a mode-locked Coherent Mira 900 F Ti/sapphire oscillator. The mode-locked Ti/sapphire produced a 76 MHz pulse train which was then trimmed to ca. 5 MHz by a pulse picker. The resulting beam had a working wavelength of 820 nm, nominal pulse duration of 200 fs and pulse energy of 10-20 nJ. This laser light was then guided through a polarizer (P1) adjusted for the transmission of p-polarized light. The laser light was focused onto the electrode surface with focusing lens L1. The second harmonic signal generated and the reflected laser light were collimated through a collecting lens (L2) of the same type as L1. The collimated beam was incident on a polarizer (P2) mounted in a holder (Oriel) which rotates perpendicular to the direction of propagation of the beam. The beam then enters a dark box and passes first through a spectroscopic cell containing a $CuSO_4$ solution (F1) and then a 410 nm narrow-band pass interference filter made by CVI Laser Corporation (F2). Filters F1 and F2 cut the 820 nm original laser light out

of the beam, leaving only the 410 nm SH signal. The SH signal is then focused onto a PMT with another focusing lens (L3). The PMT is housed in a thermoelectric cooling chamber (Princeton Applied Research, PAR) operating at ca. -20ºC. The model 1140A quantum photometer (PAR) was operated by the use of an amplifier/discriminator and a high-speed ratemeter, the ratemeter also providing the voltage required by the PMT. The analog photon counting signal was collected via a National Instruments PCI 6024E data acquisition board connected to a desktop computer. The signal was then digitized by a DAC board. Custom software built using LabView was used to control the rotation of P2 and recorded the electrochemical data for each experiment. The software collected 5 measurements for each degree of rotation of P2. The data for each rotation angle was then averaged during data processing. Experiments conducted where the SHG signal was monitored as a function of applied potential were performed with rotating polarizer P2 fixed to allow for the transmission of p-polarized light.

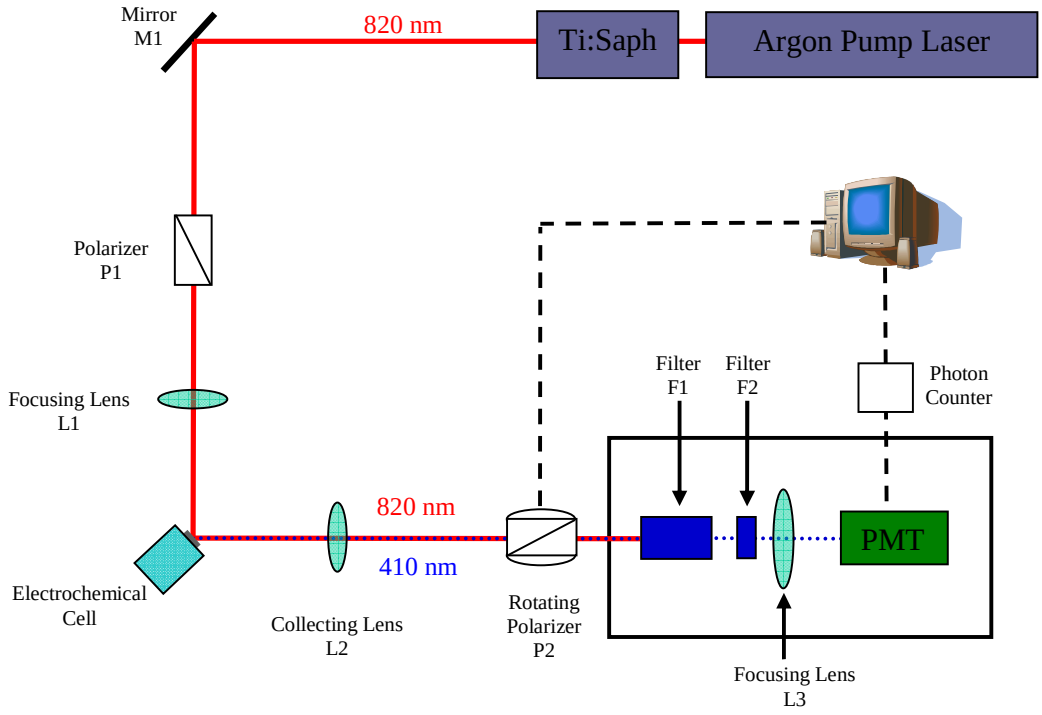

Figure 2.4 - Block diagram showing the experimental set up used for *in situ* SHG-ORD experiments

2.2.2 Electrochemical cell, equipment and electrodes

A 0.2 M solution of 99% KCl (EM Science) served as the base electrolyte in all spectroelectrochemical experiments. 99+% L-cysteine (Acros Organics), 99% D,L-Cysteine (Aldrich) or ≥98% 2-mercaptoethylamine (MEA) (Fluka BioChemika) were then added to the cell when conducting experiments. Experiments conducted with MEA were performed under pH control using a phosphate buffer system (PBS) adjusted to pH ≈ 6.5. 18.2 MΩ-cm ultrapure water used to make all electrolytes and in the cleaning of the cell and glassware was obtained from a Barnstead NANOpure Diamond water purification system. All glassware was cleaned in an acid bath

consisting primarily of concentrated sulphuric acid with a small amount of concentrated nitric acid. The electrochemical cell used for *in situ* SHG-ORD measurements is shown schematically in Figure 2.5. The body consists of a 25 mm threaded ACE glass fitting with two 7 mm glass arms attached to the sides, allowing for both a Luggin capillary and a compartment with porous frit to be inserted into the cell in close proximity to the working electrode. A Ag|AgCl|Cl^-(saturated) electrode mounted at the end of the Luggin capillary was used as a reference electrode, while a 0.3 mm platinum wire (Alfa Aesar) set in the porous frit compartment was used as a counter electrode. The working electrode was constructed from a 99.99% silver rod (Premion, Alfa Aesar) with a diameter of approximately 6.35 mm. The rod was cut into a disk and a small threaded hole was drilled into the face opposing the working surface. Electrical contact was made *via* a stainless steel rod threaded into this hole. Prior to mounting in a Teflon holder the electrode was immersed in concentrated nitric acid to oxidize it, then polished using 600, 2400 and 4000 grit emery paper, followed by 1μm, 0.3μm and 0.05μm alumina suspensions and rinsed with copious amounts of ultrapure water. The potential of the working electrode was controlled with a Hokuto Denko potentiostat/galvanostat (HAB-151) during experiments. The prepared cell was purged with pre-purified N_2 gas for 20 minutes prior to data collection, with a small stream of N_2 being bubbled through the cell throughout the entire experiment.

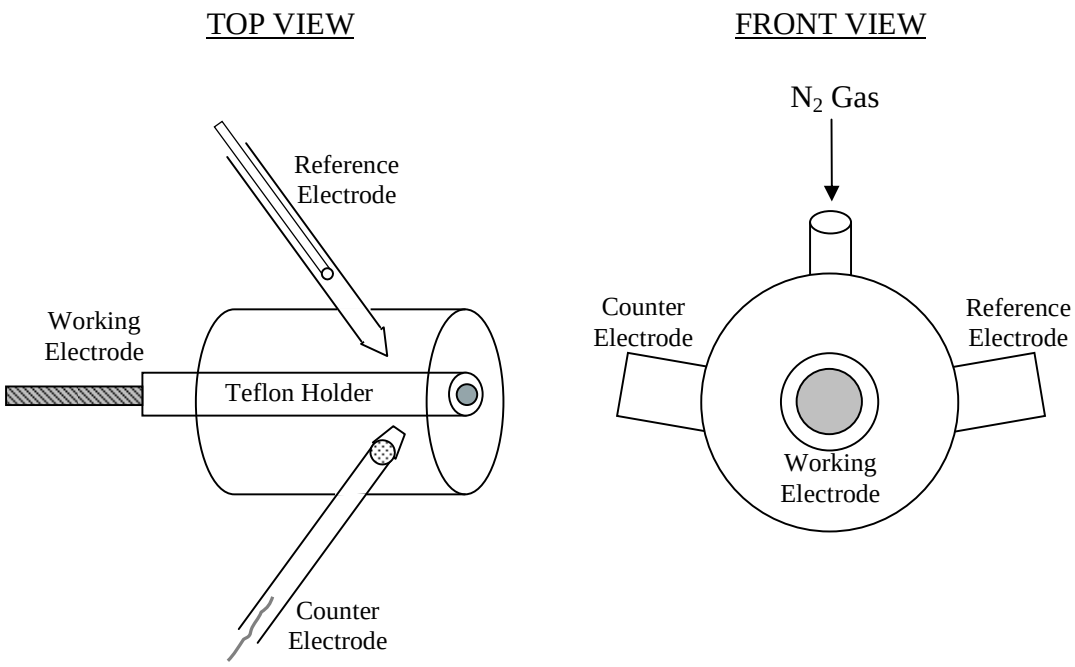

Figure 2.5 - Schematic diagram of the spectroelectrochemical cell used for *in situ* SHG-ORD experiments.

2.2.3 Data Processing

After being properly formatted in Microsoft© Excel, SHG-ORD data was processed using Vernier Software's Graphical Analysis for Windows™. This program was used to fit the collected intensity of the SHG signal to a sine squared function as related to the angle of rotation of P2 away from *p*-polarized, Ω (*Equation 2-3*)[57] . A rotation of 90° will indicate a beam composed entirely of *p*-polarized light, while 0° corresponds to a beam of purely *s*-polarized light.

Equation 2-3

$$I_{2\omega} = A[B + \sin^2(\Omega - \phi)]$$

Ω is fixed for each angle of rotation of P2, while the other variables are adjusted to provide the best least-squares fit. The value of greatest interest in these studies is ϕ, the SHG-ORD rotation angle, describing the magnitude and direction by which the polarization curve has been shifted. Under the dipole approximation of SHG ϕ should be equal but opposite for L vs. D enantiomers and zero for a racemic mixture of chiral molecules[57].

2.3 Results

In situ SHG ORD experiments were performed on a polycrystalline Ag electrode with cysteine of differing chirality adsorbed onto the optical surface in aqueous solutions. This was done towards the goal of observing a difference in the SHG-ORD rotation angle, ϕ, between the L and D form of the molecule.

All ϕ values presented in this thesis have been normalized with respect to a polycrystalline Ag electrode with no cysteine adsorbed. The experimental setup itself appears to exhibit a ϕ on its own without a chiral adsorbate introduced. This ϕ is a result of minor misalignments in the set-up and not a true rotation of polarization. Therefore it was necessary to repeat the blank Ag experiments initially, before introducing the cysteine into the system each day experiments were being performed. These initial values were then used as a reference for measuring ϕ due to adsorption of L-cys onto the Ag electrode.

As an indication to ensure that the Ag electrode was clean at the beginning of the experiment, the SHG signal was monitored with respect to the applied potential with the variable polarizer, P2, set to transmit completely *p*-polarized light. The

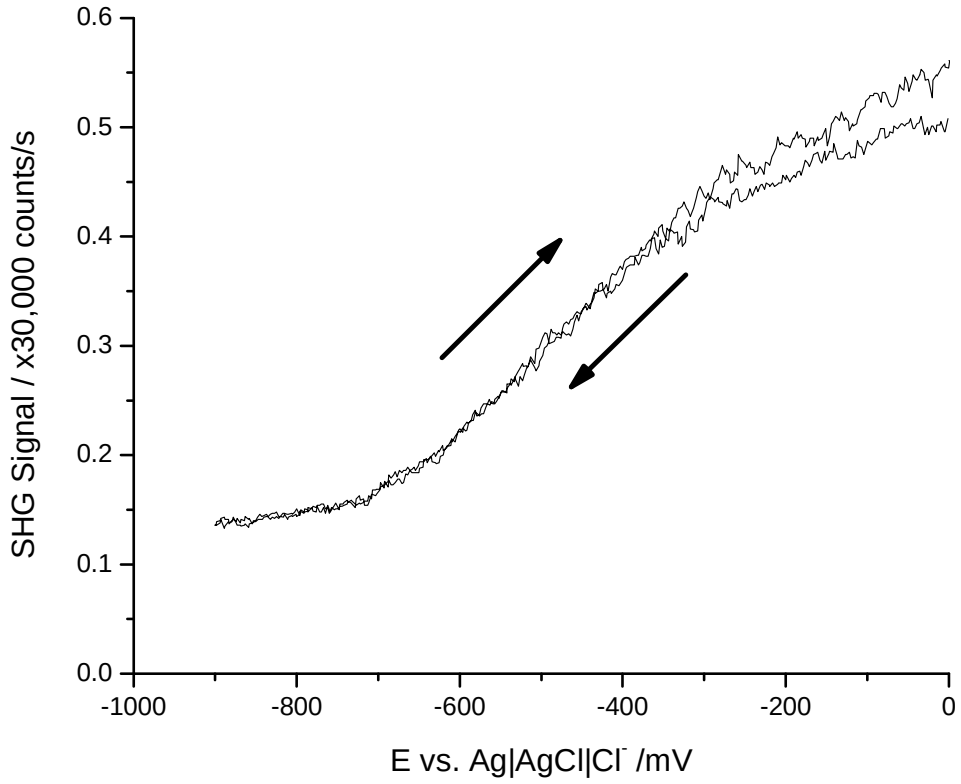

Figure 2.6 - Potential dependence of SHG signal collected from a polycrystalline Ag electrode in 0.2 M KCl. Potential scanned between 0 mV and -900 mV, starting and ending at 0mV.

resulting signal was examined to determine that the SHG signal had a parabolic shape, with the minimum occurring approximately at the potential of zero charge (pzc). The pzc for polycrystalline Ag occurs at -900 mV vs. Ag|AgCl|Cl^-(saturated).

Any unwanted adsorbate on the silver which will affect the electronic structure of the metal will change the shape of the SHG potential plot, thus indicating that a contaminant is present and must be removed. An example of a clean SHG potential plot is shown above in Figure 2.6. Once this step was completed SHG-ORD experiments were performed on the bare Ag electrode at the potentials of interest several times, obtaining an average ϕ for each potential.

Once all the bare Ag *in situ* SHG-ORD reference data was collected, the output polarizer was again set to completely *p*-polarized and the addition of cysteine into the spectroelectrochemical cell was recorded over time. This was done to ensure that the adsorption of cysteine onto the electrode surface had reached equilibrium before measurements were performed. A sample plot showing the addition of L-cysteine at a constant applied potential of -700 mV is shown in Figure 2.7. In this figure the addition of L-cysteine is clearly visible by a steep spike in SHG signal followed by a more gradual decrease until levelling off and remaining relatively constant.

In situ SHG-ORD plots were then obtained by fixing the applied potential and measuring the intensity SHG signal as polarizer P2 was rotated. As can be seen in Figure 2.8 the resulting SHG-ORD plots contain a vast amount of data (5 data points per degree of rotation) and fit the sine squared shape predicted by Byers *et al*.[57] Both the original collected data (Figure 2.8) and the resulting fitted data (Figure 2.9) are shown for comparison purposes.

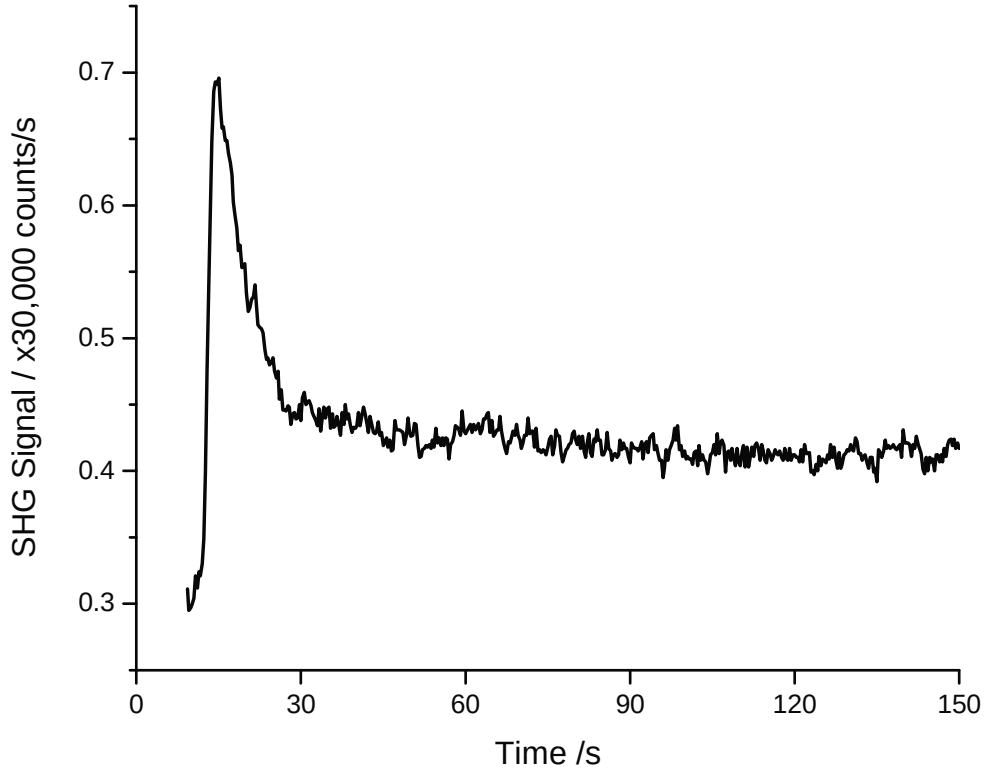

Figure 2.7 - Adsorption of L-Cys onto a polycrystalline Ag electrode at -700 mV vs. Ag|AgCl|Cl^-(saturated) as monitored by SHG.

Upon visual inspection of Figure 2.8 and Figure 2.9 it is clear that the maxima of the SHG-ORD plots are shifted away from their natural position at 90º. That the bare Ag exhibits a rotation angle highlights that the experimental setup used has some minor misalignments. All shifts reported in this work were therefore measured relative to the bare Ag electrode. It is also evident that adsorption of cysteine onto the Ag electrode surface results in a change in ϕ with respect to the bare Ag electrode.

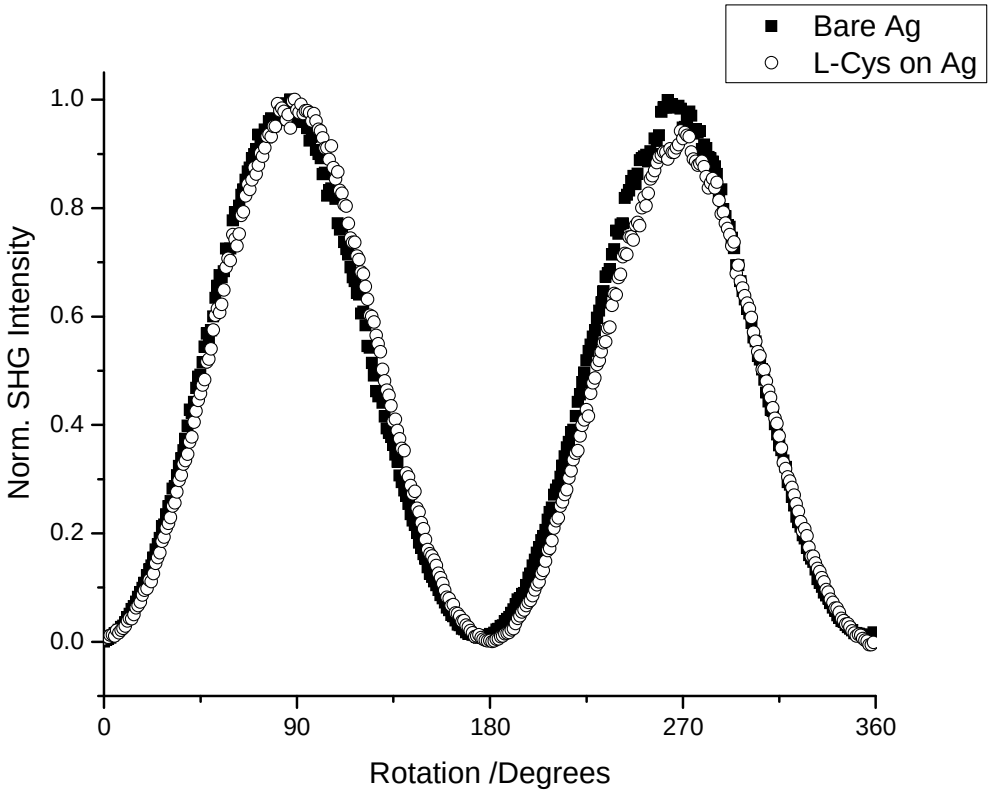

Figure 2.8 – *In situ* SHG-ORD plots obtained from the surface of a polycrystalline Ag electrode at -700mV vs. Ag|AgCl|Cl^-(saturated). The experiments were run in the presence (○) and absence (■) of L-Cys adsorbed on the surface.

In situ SHG-ORD experiments were performed for L- and D-cysteine as well as the racemate at -100 mV potential intervals starting at -700 mV. These experiments were performed in 0.2 M KCl solutions, therefore the potentials were selected such that the coadsorption of Cl^- on the Ag electrode is minimized. Cl^- is expected to desorb from a polycrystalline Ag electrode around -650 mV[11].

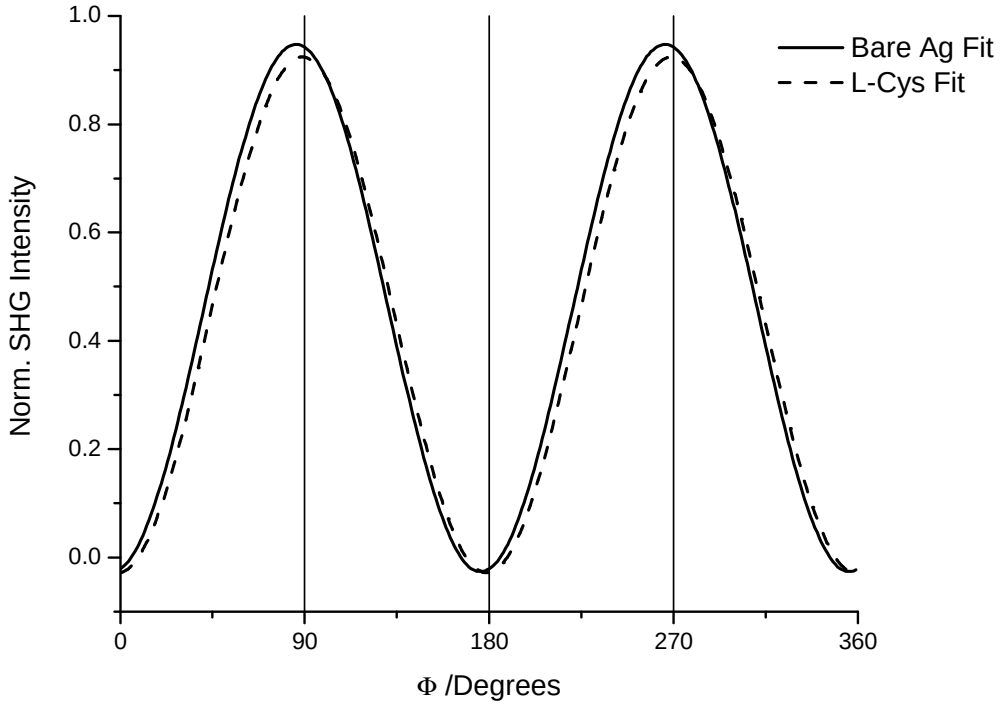

Figure 2.9 – Theoretical fit for the experimental data in Figure 2.8 in the absence (——) and presence (------) of L-Cys.

All *in situ* SHG-ORD data collected for each enantiomer at each potential was combined together and has been presented in Figure 2.10. The error bars presented in the plot represent a 95% confidence interval. There are several important characteristics to be noticed and discussed in Figure 2.10. Firstly is that all forms of cysteine studied exhibited negative ϕ values. This was somewhat unexpected from the theory proposed by Byers *et al.* and seems to be in discord with the results of Kadodwala *et al*. in their study of cysteine on gold.

It was expected that similar results to Kadodwala *et al* would be obtained, due to the similarity of the properties of Ag and Au and that the analyte molecule was the same. Upon first examination, this does not appear to be the case. All of the ϕ values had the same sign and different magnitudes. It was expected that the magnitudes of ϕ for the L- and D-cysteine enantiomers would be the same, while the sign would be opposite between the two. The racemate was expected to exhibit a ϕ of 0°.

The other characteristic of note in Figure 2.10 is that generally the ϕ of the racemate fell between those of the two enantiomers, with the L-cysteine shifting to more negative values of ϕ than D-cysteine. This behaviour espouses the idea that a chiral signal is possibly being observed alongside contributions from one or more other sources. There are several possibilities of sources which could be contributing to the rotation angle observed in these studies. The electronic and magnetic structure of free-electron metals leads to several sources of SHG from metal surfaces, as discussed in Section1.5.2. It is likely that the electric dipole term is not solely responsible for the SHG signal generated from the Ag surface. The additional electric quadrupole and magnetic dipole terms could therefore be contributing to the consistently negative ϕ values observed for cysteine.

The uniformity of the sign of the ϕ values obtained for cysteine could also be related to a resonance effect. Although cysteine does not have an absorption peak at either 820 nm or 410 nm, the Ag substrate does have an absorption band in the

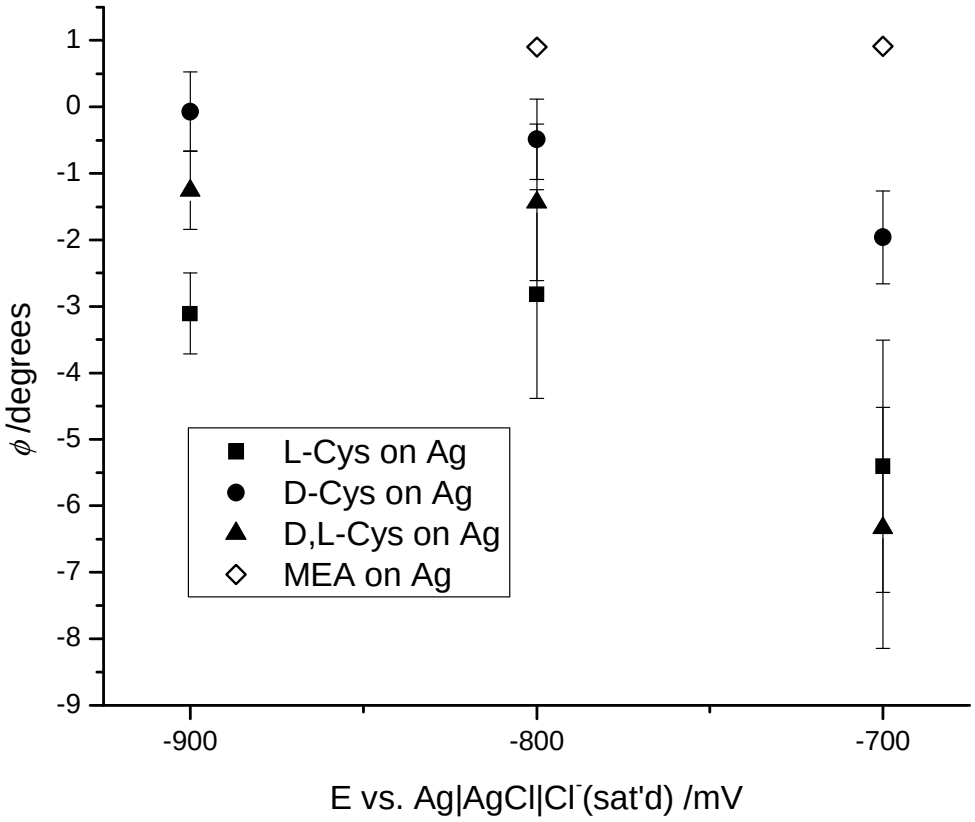

Figure 2.10 – *In situ* SHG-ORD rotation angles ϕ for MEA, L-Cys, D-Cys and D,L-Cys adsorbed on polycrystalline Ag.

vicinity of the 410 nm SHG wavelength. The reflectivity of a polished Ag surface drops to a minimum at approximately 330 nm, with the decrease beginning at approximately 490 nm[63]. As SHG can be resonance enhanced, this absorption band could be resulting in an effect on ϕ. The experiments performed however do not allow for the distinction between which of these mechanisms or which combination of mechanisms would result in the effects observed.

In an effort to gain further insight into the processes at play, *in situ* SHG-ORD experiments were performed on 2-mercaptoethylamine (MEA). MEA has the same chemical structure as cysteine except that is achiral due to the lack of the carboxylic acid group. It was hoped that a similar molecule with no chirality would clarify the results obtained from cysteine. Unfortunately instrument repairs and delays as well as alignment problems hindered the collection of SHG-ORD plots for MEA on Ag, and as a result data from only one day were used.

The results from these experiments are represented in Figure 2.10 by the open diamond markers. The MEA was observed to have a small positive rotational angle. This shift does not provide any new insight into the link between the ϕ values observed for cysteine and the chirality of cysteine. It does however further highlight the belief that more than the optical activity of cysteine is contributing to ϕ.

The last attribute of Figure 2.10 of note is that the order of the ϕ values for the cysteine enantiomers at each potential seem to become more clearly chiral as the potential is made more negative. At -700 mV there is little to no difference between the rotational angles of the SHG-ORD plots for the three forms of cysteine, however at -900 mV, there is little overlap between the three data sets and the racemate is very nearly centred between the L- and D-enantiomers. This seems to support the idea that the coadsorbed Cl^- is likely contributing to the effects observed. Not surprisingly it is therefore evident that as more and more Cl^- desorbs from the Ag electrode surface, the expected chiral distribution becomes more clearly defined.

2.4 Summary and Conclusions

The imprinting of the chiral signature of an adsorbate onto the electronic structure of a metal substrate has been previously observed. However the adaptation of this method to an *in situ* electrochemical interface is shown here for the first time.

A method where the electronic structure of a metal can be probed is quite useful for several different applications, most notably for heterogeneous catalysis. The development of this technique is therefore beneficial towards the fundamental understanding of enantiospecific processes occurring at metal interfaces.

This study determined that a chiral moiety adsorbed at a metal surface can imprint its optical activity onto the electronic structure of the substrate, as demonstrated with a cysteine/Ag system. However, it is likely that other processes which are occurring concurrently with the chiral perturbation are also contributing to the collected signal.

Therefore further studies would be recommended to more fully develop the origins of the SHG signal which was observed in *in situ* SHG-ORD experiments which were performed. It would be particularly useful to repeat the *in situ* SHG-ORD experiments with MEA on polycrystalline Ag, as well as adding 3-mercaptopropionic acid (MPA) to the cell, to ensure that the MEA results are not merely coincidental. Performing *in situ* SHG-ORD experiments under pH control as well could provide further insight into this process, as it is likely to affect the composition of the

overlayer structure, and would possibly result in a change in the rotational angle observed from the system.

Chapter 3 - *In Situ* SERS of L-Cysteine on Polycrystalline Ag

This chapter presents the results of *in situ* SERS experiments characterizing L-cysteine adsorbed on polycrystalline Ag at basic, neutral and acidic pHs. An introduction highlighting the relevant studies performed using both solution Raman and SERS opens the chapter. It is then divided into two separate sections, the first describing the materials, methods and results of solution Raman experiments and *ab initio* calculations performed, while the second describes the *in situ* SERS experiments conducted. The results from the first section are used as a basis for the interpretation of results obtained in the second part. *In situ* SERS experiments were used to propose an adsorption geometry for L-cys on Ag under different pH and potential conditions. The results for both sections are summarized in the final section.

3.1 Introduction

The vibrational spectrum of a molecule can be very useful in the elucidation of chemical and structural properties. Raman spectroscopy has therefore found great success in the study of chemical systems, as discussed in Sections 1.6 and 1.7 .

The study of amino acids is of great interest for many different reasons, from modeling of proteins to exploitation of their functionality. As such they have been extensively studied, and L-cysteine is no exception.

.

The normal Raman spectrum of crystalline L-cysteine and L-cysteine in aqueous media has been repeatedly studied both experimentally and

computationally[64-67]. Part of the original appeal for the studies conducted with L-cysteine is that it is a small molecule with several functionalities. This makes L-cysteine adaptable to many different systems, and hopefully a more tractable assignment of bands from the vibrational spectrum. In practice, however, the small size and lack of symmetry make vibrational analysis difficult. Many of the vibrations are coupled together making the correct assignment of vibrational bands to specific functional groups challenging. Deuterium exchange experiments have also been used to gain insight into the vibrational fingerprint of L-cysteine[66]. Surprisingly there are no studies showing the effect of pH, and thus protonation, on the vibrational spectrum. This approach should be able to provide valuable data towards refining the vibrational profile of L-cysteine.

Perhaps of greater importance is the characterization of adsorbed L-cysteine. L-cysteine readily attaches to certain metallic surfaces, such as Ag, which can be used in many different applications. Fundamental studies probing the manner in which the molecule adheres to the surface are therefore of great interest to the scientific community. As such, several studies have been conducted in the pursuit of this end *via* SERS experiments[11,68,69]. It is agreed that there are three main conformations in which L-cysteine can adsorb onto a metal surface, as depicted in Figure 3.1. These conformations show the strong Ag-sulfide bond being the constant linkage to the surface, with the amine and carboxyl groups interacting with the surface to varying degrees.

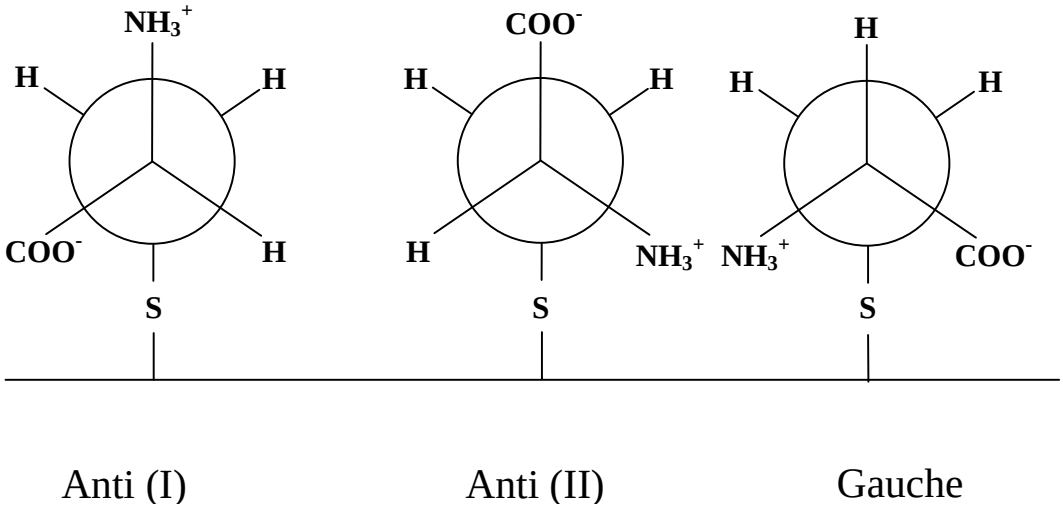

Figure 3.1 - Newman projections showing the possible conformations of adsorbed L-cysteine, reproduced from[11].

Jing and Fang conducted SERS experiments looking at the adsorption of L-cysteine on gold and silver nanoparticles[68]. They determined that L-cysteine adsorbs on gold nanoparticles in the gauche configuration. In the case of silver nanoparticles they observed the formation of L-cystine dimers adsorbed to the surface, as well as L-cysteine molecules adsorbed in the gauche and anti (I) configuration. This result was only observed when chloride was added to the silver colloid, causing agglomeration of the nanoparticles and an enhancement of the SERS effect[68].

Although these results are interesting, it is more useful from an applicability perspective to study a simple metal surface under potential control. Brolo *et al.* conducted potential dependent SERS experiments of L-cysteine adsorption on to a polycrystalline electrode at neutral pH in a KCl electrolyte[11]. This study analyzed

only the low frequency region of the Raman spectrum between 500 cm^{-1} and 950 cm^{-1}. This study provided valuable insight into the configuration of the L-cysteine adsorbed at the silver surface and its subsequent potential induced re-orientation. It was proposed that at potentials more positive than -650 mV an anti (II) conformation dominates, with the carboxyl group pointing away from the surface and the amine interacting with the surface stabilized by adsorbed chloride. At potentials more negative than -650 mV chloride desorption occurs and a re-orientation of the adsorbed molecule to an anti (I) configuration was observed[11].

While the study by Brolo *et al.* was important, the narrow frequency range studied allowed only for the examination of the vibrations associated with the carboxylate group and the C-S stretch. Graff and Bukowska[69] performed a study examining both lower and higher frequency Raman bands. In addition, they varied the pH of the electrolyte, thus controlling the protonation of the L-cysteine molecule. This could provide additional valuable data concerning the configuration of the molecule adsorbed at the Ag surface, as electrostatic interactions would be expected to play a significant role in the adsorption geometry. However, this study was directed towards the determination of chiral effects on the SERS spectrum of enantiomeric and racemic cysteine. This study did indicate that at acidic pH at potentials more positive than -800 mV or -700 mV (for pH=2 or pH=3 respectively) L-cysteine adsorbed primarily in the gauche configuration, and that an anti (II) configuration is favoured at more negative potentials[69]. This study was important in understanding the details of L-cysteine adsorption on Ag surfaces; however

experiments providing details on the effect of pH and applied potential on adsorption geometry would still be beneficial in the understanding of the system as a whole.

3.2 Solution Raman of L-cysteine in aqueous media at various pH

3.2.1Experimental

Instrumentation

Solution Raman spectra were collected using a Renishaw inVia Raman microscope system with a Renishaw 632.8nm HeNe laser as excitation source. The laser was focused into the solution with a 63x Leica water immersion microscope objective (NA=0.90). The Raman microscope functions in back-scattering mode with the same objective used for excitation and collection. The laser was focused into the sample solution by immersing the microscope objective into the solution.

Optical Cell and Solutions

All water used in the preparation and cleaning for Raman experiments was 18.2 MΩ-cm ultrapure water from a Barnstead NANOpure Diamond water purification system. All glassware used was cleaned in an acid bath consisting primarily of concentrated sulphuric acid with a small amount of concentrated nitric acid. The cell used was a simple block of Teflon with an approximately 3/4” diameter hole bored through it. The bottom of the cell was sealed with a 1”x1” gold slide pressed up against a rubber O-ring inset into the base, gold side down. The cell was cleaned in a piranha solution composed of 3 parts concentrated sulphuric acid and 1 part 30% hydrogen peroxide when solutions were changed.

All solution Raman spectra were collected from a solution of 1.0 M L-cysteine (99+%, Acros organics). Neutral conditions with pH of ~6 were generated by making up the cysteine solution in 0.1M KCl (99%, EM Science). Acidic conditions with pH of 2 were generated by making up the cysteine solution in 0.1M KCl (99%, EM Science) acidified with sulphuric acid. The pH of the acidified KCl was determined using an Orion Model 420 pH meter. Basic conditions with pH of 13 were generated by making up the cysteine solution in 0.1M NaOH (≥97%, ACP).

3.2.2 Results

To aid in the determination of the Raman bands observed in SERS spectra of L-cysteine (L-Cys) adsorbed on silver at various pHs, the solution Raman spectrum for L-Cys at various pHs was collected.

The assignment of the Raman peaks in these spectra was completed with the aid of a DFT calculation of the L-cysteine zwitterion, where the amino group is protonated and the carboxyl group is deprotonated. This calculation was performed using Gaussian 03W® at the B3LYP level using a 6-311G(d) basis set and using the IEFPCM water solvation model. The vibrational frequencies and their proposed band assignments are listed in Table 1. These assignments are based on observation of the vibrations in GaussView and previous band assignment from the literature. It should be noted that *ab initio* calculations generally result in values with a 10-15% difference compared to experimental values.

Table 1 also contains experimental data collected for solutions of L-Cys at different pHs. The full Raman spectra for each pH are shown in Figure 3.2. The change in pH results in a change in the protonation of L-Cys, as shown in Figure 1.2. In more symmetrical molecules a change in protonation state can lead to changes in the overall molecular symmetry. This might result in a relaxation of the selection rules for Raman scattering and drastic changes in the vibrational bands. Cysteine however, is not a symmetrical molecule, and thus protonation will not result in the complete loss of a band or a clear generation of a new peak. Smaller changes in the spectrum can be observed though. The mass change resulting from the gain or loss of a proton can cause a frequency shift for certain bands. Considering the classical model, it is expected that the addition of a proton will produce a frequency shift towards lower energy, as the bond will vibrate at a lower frequency, while the loss of a proton will increase the energy of the vibration and the band will be observed at a higher frequency.

Table 1 - Theoretical and experimental frequencies of L-cysteine at different protonation and their assignment based on literature[65,68,69] and calculations.

Theoretical Calculations		Experimental Results		
L-Cysteine zwitterion	Band Assignment	Acidic L-Cysteine	Neutral L-Cysteine	Basic L-Cysteine
482	CCN bend	473	476	464
	Artefact			497
	S-S stretch	532	528	531
662	CS stretch	683	684	684
768	CH2 rock	779	778	782
799	C-SH bend	816	816	817
849	C_a-COO- stretch*	874	875	874
899	HCN bend + HCH bend	936	936	936
985	NCH bend + HCH bend	981	995	995
1062	HCH rock + NCH bend	1063	1066	1065
1236	CO stretch + HCN bend	1214	1213	1213
1298	CCH bend	1310	1310	1310
1320	CH_2 twist + HNH bend	1350	1350	1350
1383	C_aC_b stretch + CH bend + COO^- symm. stretch	1400	1400	1401
1451	CH2 bend	1428	1429	1428

* C-C_α-C_β-S

The pH conditions used in the solution Raman experiments were designed to result in full protonation of the molecule for acidic conditions (pH = 2), partial protonation for neutral conditions (pH ≈ 6) and full deprotonation for basic conditions (pH = 13). The true states of L-Cys in these solutions is not likely to be quite as clear cut as this model, though the trend does apply. The acidic pH of 2 is fairly close to the pK_a of the carboxyl group, and therefore is most likely only partially protonated. The neutral conditions are close to the pK_a of the amino group, though there is a large enough difference that the majority of the amino groups should be protonated. The basic conditions, on the other hand seem to be extreme enough to fully deprotonate all three groups.

Comparison of certain bands associated with each of the functional groups in L-Cysteine support this analysis. It should first be noted that the strong low frequency band found at 497 cm^{-1} under basic conditions in Figure 3.2 is an artefact and does not represent a vibrational mode of L-cys.

The NCH bending + HCH bending mode shows a good correlation to this trend. The frequency of the band varies from 981 cm^{-1} under acidic conditions to 995 cm^{-1} under basic conditions. Since under basic conditions the amino group will be deprotonated it is expected that it will vibrate with a higher frequency. A similar trend is also evident in the C_α-C_β stretch + CH bend + COO^- symmetric stretch observed around 1400 cm^{-1} and the C-SH bend observed around 816 cm^{-1}.

There are also several bands which might be expected to show a similar trend, but did not. However, from careful consideration of the processes at work it can be seen that the proposed model still remains true. Several of the bands which did not follow the expected pattern were found at 936 cm^{-1} and 1063 cm^{-1} and 1214 cm^{-1}. Visual observation of the vibrations shows that the coupling of vibrations from different functional groups of the molecule could mask the expected trends in these cases. The other notable exception to the trend was the C_{α}-COO^{-} stretching band around 875 cm^{-1}. It could be expected that the protonation state of the carboxyl group would result in a shift in the frequency of this band, however no change is observed as pH varies. This phenomenon can be explained by looking at the proximity of the proton in question to the actual bond which is characterized by the vibration. It is evident that the proton is not directly attached to either end of the C-C stretching, and thus would likely not have a large impact on the frequency of the vibration.

The band assignment proposed for the solution Raman spectra collected seems to agree well with the expected effect protonation would have on the vibrational profile of L-Cys. This assignment will provide a good foundation, allowing for the interpretation of SERS spectra of L-Cys adsorbed on a Ag electrode.

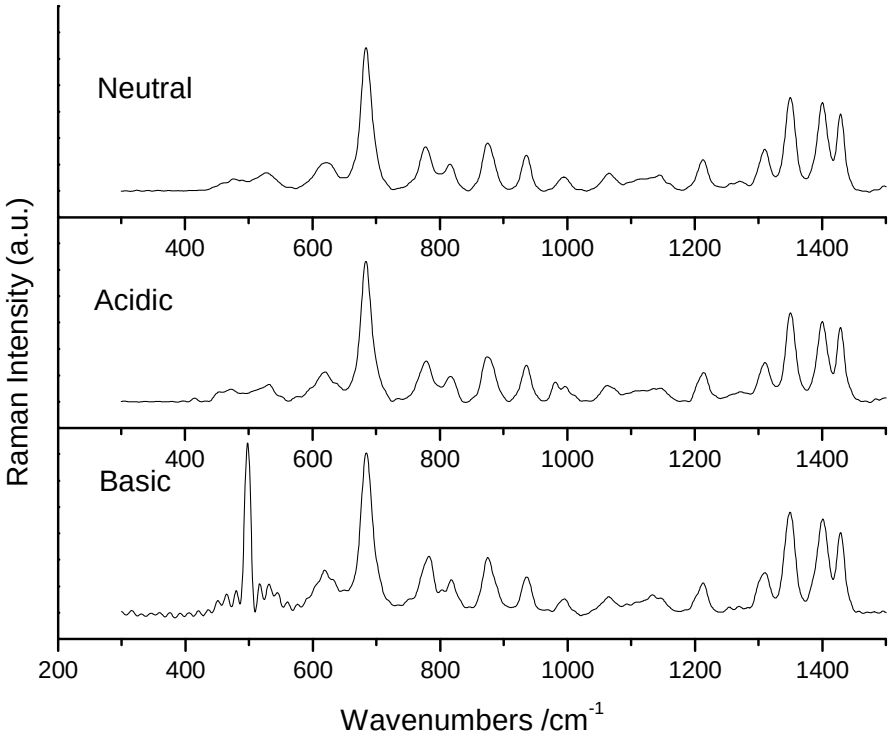

Figure 3.2 - Solution Raman spectrum of L-cysteine in acidic (pH=2), neutral (pH ≈6) and basic (pH=13) conditions.

3.3 *In situ* Surface Enhanced Raman Scattering (SERS) of L-cysteine adsorbed at polycrystalline Ag at various pH

3.3.1 Experimental

Spectroelectrochemical cell

A side-view of the spectroelectrochemical cell used for *in situ* SERS experiments is shown in Figure 3.3. The main body of the cell consists of two Teflon pieces sandwiched together with two screws, with a rubber O-ring between them to prevents leaks. The top piece has a 3/4" hole bored through its centre, while the bottom has a smaller hole designed for the passage of the Teflon rod holding the electrode. The electrode was a disk of approximately 6.35 mm diameter with a small threaded hole in the end opposite the working face. Electrical contact was made *via* a stainless steel rod threaded into this hole. The electrode and stainless steel rod were mounted in a Teflon rod so as to electrically isolate the electrode, excluding the working face, from the electrolyte. Electrolytes used were as prepared for the solution Raman experiment with the exception that the concentration of the L-cysteine solutions were 0.1 M, not 0.3 M. A platinum wire inset into the circumference of the large hole acted as a counter electrode, while a Ag|AgCl wire acted as a reference. The reference electrode was normalized by measuring its potential relative to a Ag|AgCl|Cl^-(saturated) reference electrode in each solution, with final potentials being adjusted accordingly.

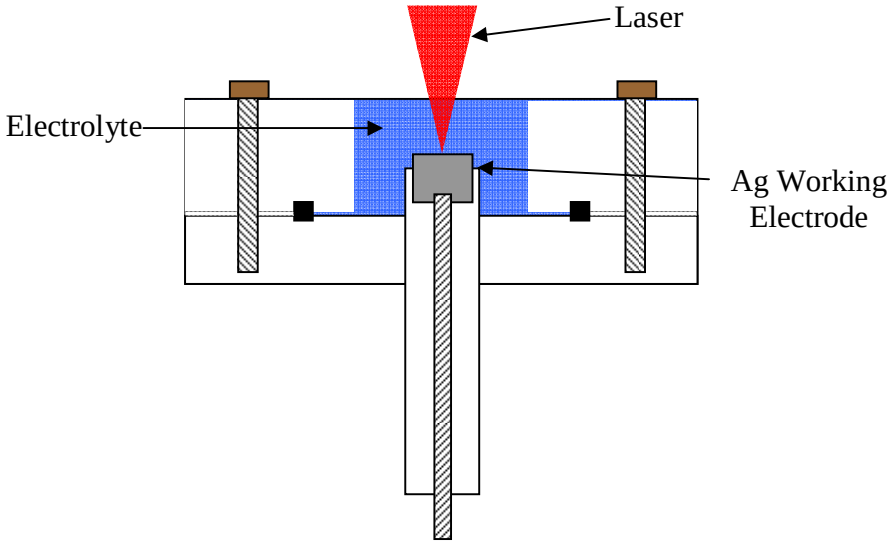

Figure 3.3 - Side-view of spectroelectrochemical cell used for *in situ* SERS experiments.

Electrode Activation

The polycrystalline Ag electrode used as the working electrode in SERS experiments was the same as that used for SHG experiments which were described in Chapter 2. The electrode was roughened electrochemically by running oxidation/reduction cycles to create a SERS active surface. The first step of the procedure was to oxidize the working surface of the electrode with concentrated nitric acid and then polish it. This was done with 600, 2400 and 4000 grit sandpaper, followed by polishing with 1μm and 0.3 μm alumina suspensions. The electrode was then mounted into the cell as depicted in Figure 3.3 with 0.1 M KCl added as electrolyte. The cell was connected to an Autolab PGSTAT 30 potentiostat/galvanostat. The potential was then scanned from -300 mV to +125 mV, 25 times at a 20 mV/s scan rate, to oxidize and reduce the silver, creating a rough

surface. Measurements were then performed by replacing the KCl solution with a solution containing L-Cysteine.

Instrumentation

In situ SERS experiments were collected from a custom built Raman microscope. A He-Ne laser (Melles Griot) was used to produce the 632.8 nm excitation source. An Olympus BHT microscope outfitted with an Olympus long working distance 50x objective (NA=0.55) was used to focus on the surface of the working electrode. The system operated in back-scattering mode, thus the objective used for excitation was also used for collection. The scattered light was then filtered with a Kaiser super notch filter to remove the Rayleigh scattered light. The remaining light was then directed through a Kaiser Holospec f/1.4 spectrograph coupled with an Andor CCD detector (model DV-401-BV) where the Raman spectrum was detected. A schematic depicting the experimental set-up is shown in Figure 3.4. The electrode potential during *in situ* measurements was controlled *via* a Princeton Applied Research Model 173 potentiostat/galvanostat.

Cyclic voltammetry (CV) experiments were performed in the spectroelectrochemical cell using the same set-up as for electrode activation. The CVs were collected from a smooth Ag surface in the same electrolytes as for solution Raman and SERS experiments with 0.1 M L-Cys present in the electrolyte. The potential was scanned from 0 mV to -1500 mV with a scan rate of 40 mV.

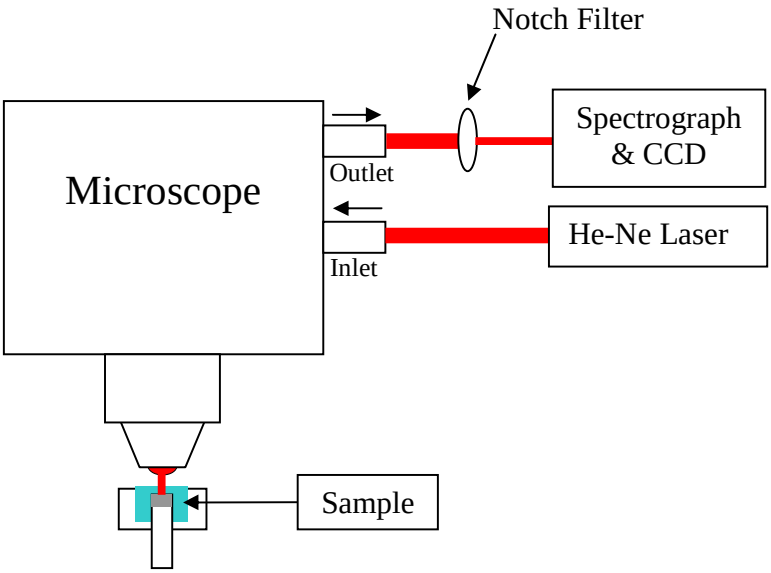

Figure 3.4 - Schematic of Raman microscope in back-scattering mode.

3.3.2 Results

SERS is a powerful tool in the qualitative determination of the adsorption geometry of molecules on a substrate. Understanding the enhancement mechanisms and the surface selection rules can provide the experimenter with valuable insight into the interaction of the adsorbate with the substrate. These principles will be utilized in this chapter to offer an explanation for intensity changes observed when the applied potential is varied during *in situ* SERS measurements of L-cys adsorbed at a polycrystalline Ag surface.

Both the EM and CT mechanisms could lead to intensity changes in the SERS spectrum of a molecule as the applied potential is changed. Changing the applied potential will change the Fermi level of the metal substrate, thus possibly moving the

Fermi level into or out of resonance with the exciting laser, effectively turning the CT enhancement on and off. In the system studied in this work it is also possible that the adsorbed Cl^- anion affects whether or not a CT mechanism is observed. The data collected is not sufficient to determine whether or not a CT mechanism is present however.

Further experiments where the coadsorbed ion is varied could aid in determining whether or not a CT enhancement mechanism is present. For example, if the coadsorbed Cl^- is leading to a CT enhancement, conducting the SERS measurements in KBr and KI electrolytes would alter the CT mechanism. Another way to determine whether a CT mechanism is occurring would be to change the excitation wavelength. If a CT mechanism is present, the enhancement will be related to the energy of the complex formed between the L-cysteine and the Ag. Changing the wavelength of the excitation laser will therefore disrupt the resonance between the CT complex and the laser, and consequently a decrease in SERS intensity will be observed.

The spectra collected in this study were interpreted assuming that the more prevalent and stronger EM mechanism is the source of the observed enhancement. There are two main principles used to elucidate adsorption geometry from SERS intensity changes under the EM model. First of all is that SERS enhancement decreases as distance from the surface increases. A simple approximation shows that the SERS enhancement for a molecule distance *d* away from a spherical surface with radius *r* scales according to G in *Equation 3-1*[70].

Equation 3-1

$$G = \left[\frac{r}{(r+d)} \right]^{10}$$

More detailed descriptions of this relationship taking into account dielectric constants and wavelength of incident light were presented by Moskovits[71,72]. The results all imply the same relationship however, that the observed SERS enhancement decreases rapidly the further the analyte molecule is from the SERS active surface.

The second principle in determining the orientation of adsorbed molecules on a SERS substrate is related to the induced dipole of the vibration. The SERS effect is observed to enhance only vibrations which have a component of the induced dipole perpendicular to the surface[71,72]. Thus a change in the SERS intensity is observed for a vibrational band when a molecular re-orientation results in an induced dipole switching from either a parallel or slanted geometry to a perpendicular geometry with respect to the surface.

Neutral Conditions

In this study SERS spectra were collected from a polycrystalline Ag electrode with L-cys adsorbed at the surface in electrolytes with acidic, neutral or basic pH. For each set of pH conditions spectra were collected from 0 to -1000 mV vs. a Ag|AgCl reference electrode at 100 mV intervals. Results from experiments performed in

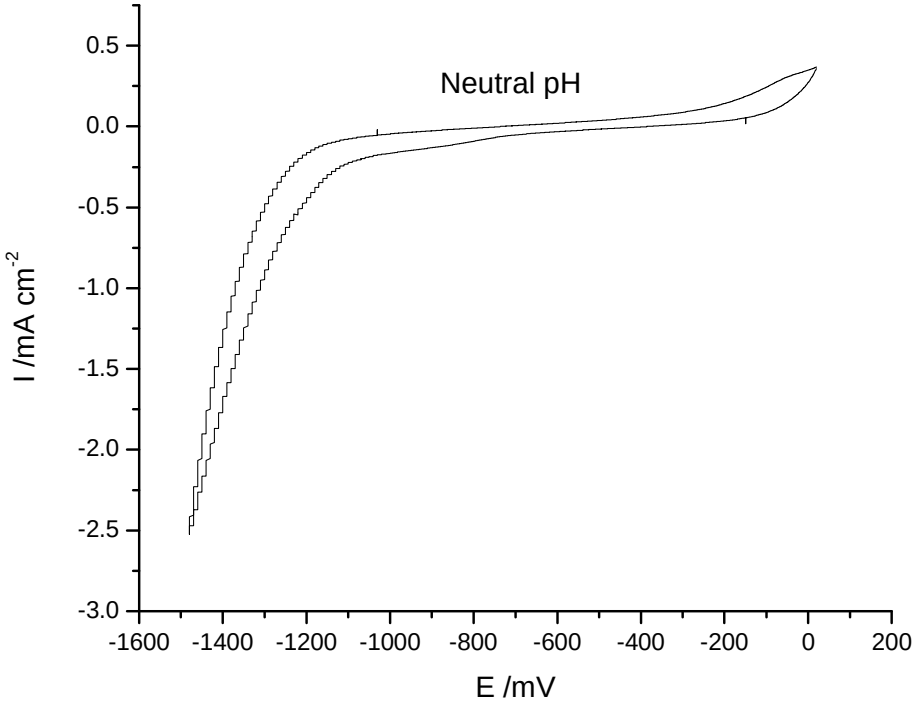

Figure 3.5 - Cyclic voltammogram of polycrystalline Ag in 0.1M L-Cys and 0.1M KCl, pH ≈6 as measured against a Ag|AgCl reference. Sweep rate = 40mV/s, 0.3mV steps in staircase potential ramp.

neutral electrolyte (pH ≈ 6) will be presented first, followed by results collected in acidic electrolyte (pH = 2). The data collected in basic electrolyte (pH ≈ 12) are not discussed in this work due to difficulties in the assignment of the observed peaks, the data collected is included in Appendix A.

To determine what effect the applied potential had on the analyte molecule, cyclic voltammograms (CVs) were collected over the potential range of interest.

Figure 3.5 shows that L-cys is stable from -200 to -1100 mV, with no desorption or reductive destruction of L-cys occurring in this potential range. The features in this CV can be attributed to the oxidation of the Ag surface at potentials more positive than -200 mV and the cathodic damaging of the Ag surface at potentials more negative than -1100 mV. This indicates that changes in SERS intensity over the potential range studied should be attributable to changes in orientation of the molecule and not to electrochemical (faradaic) processes.

The complete set of *in situ* SERS spectra collected are plotted in Figure 3.6. There are a couple of key aspects of the system being studied which are likely to contribute to the adsorption geometry of L-cys on the electrode surface.

Firstly, it is known that Cl^- adsorbs onto Ag. The presence or absence of coadsorbed Cl^- ions at the electrode surface will affect the adsorption geometry of the L-cys molecules. It has been observed that Cl^- desorption from a Ag electrode begins to occur at approximately -650 mV[11,69].

Also of importance is the point of zero charge (pzc). The pzc of a metal is the potential at which the charge density of the metal is zero *i.e.* the surface is neither positively nor negatively charged. The pzc of polycrystalline Ag occurs at -900 mV vs. Ag|AgCl|Cl^-(saturated). This is significant since it indicates that at applied potentials more positive than -900 mV the electrode will be positively charged.

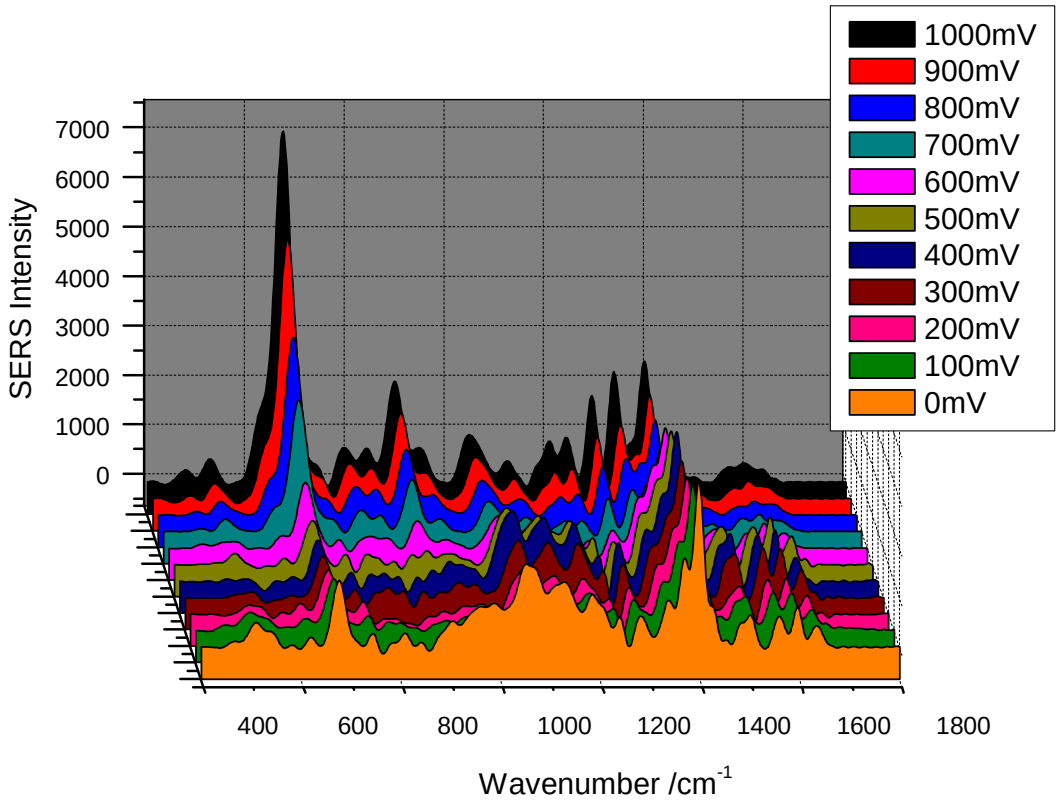

Figure 3.6 – *In situ* SERS spectra of L-Cys adsorbed at a polycrystalline Ag electrode in 0.1M KCl, pH ≈6. All applied potentials are negative vs. Ag|AgCl.

Analysis of *in situ* SERS spectra collected indicates two different adsorption geometries of L-cys which are potential dependent. At more positive potentials, greater than -600 mV a Gauche conformation with the amino groups stabilized by the Cl^- ions is expected. At potentials more negative than -600 mV, Cl^- desorption occurs and a conformational change to L-cys adsorbed in an Anti(II) configuration is observed as shown in Figure 3.7.

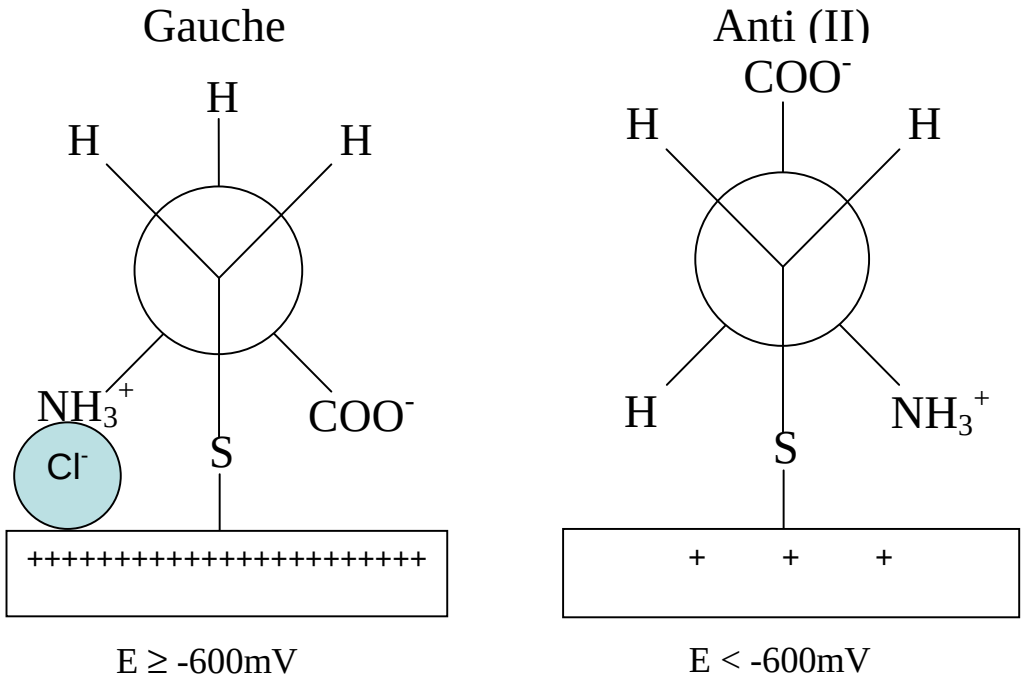

Figure 3.7 - Newman projections showing the adsorption geometry of L-cys on Ag in 0.1M KCl, pH ≈ 6.

There are four Raman peaks which were found to be of use in the determination of adsorption geometry of L-cys in neutral KCl electrolyte. Of these four peaks two were in the low frequency range between 600 cm^{-1} and 1000 cm^{-1} (Figure 3.8) and two were in the higher frequency range between 1300 cm^{-1} and 1500 cm^{-1} (Figure 3.9).

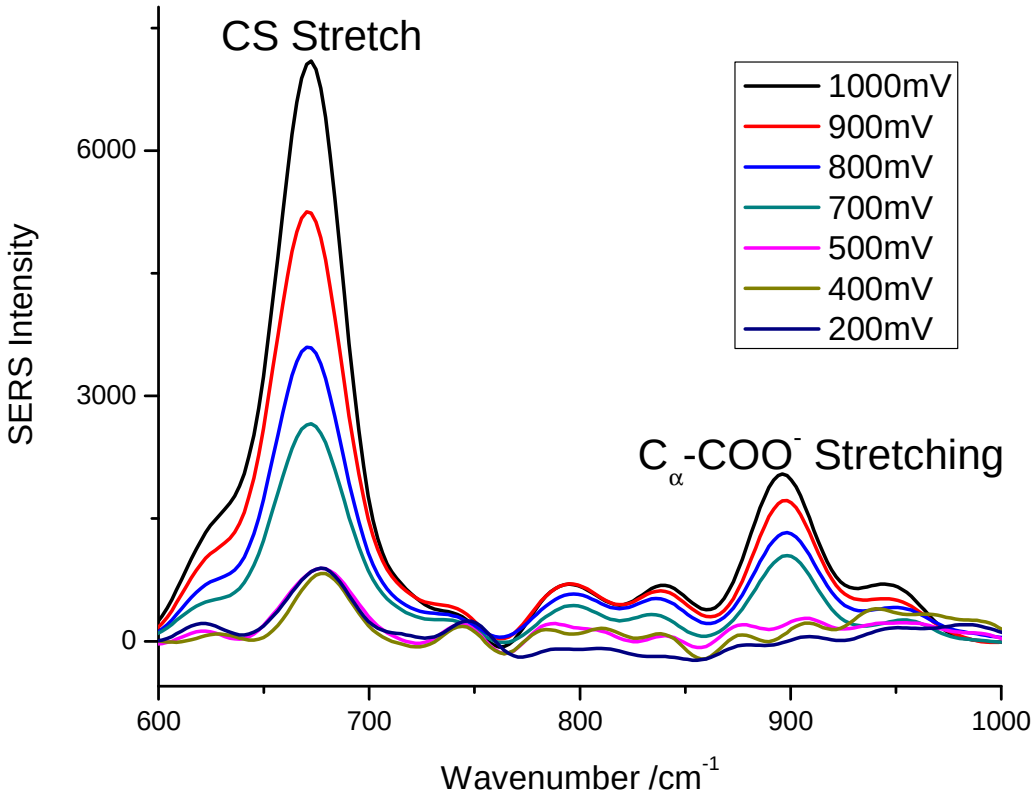

Figure 3.8 – CS and C_α-COO^- stretching bands of SERS spectra of L-Cys adsorbed at a polycrystalline Ag electrode at selected potentials vs in 0.1M KCl, pH ≈6. All applied potentials are negative vs. Ag|AgCl.

One of the most relevant peaks in this analysis is the CS stretching mode observed at 675 cm^{-1}. This peak is important for two reasons. First of all the peak is shifted to a lower frequency compared to the solution Raman spectrum, indicating that the L-cys is adsorbed on the Ag surface. This phenomenon is expected from the literature and can be attributed to the withdrawal of electron density from the C-S bond as a result of the Ag-S linking[69]. Secondly the CS stretching band shows a large increase in intensity at potentials where Cl^- desorption occurs (E<-650 mV), while the

intensity remains constant at potentials where Cl^- is strongly adsorbed to the surface (E>-650 mV). This trend can be explained by taking into consideration the Cl^- stabilized amino group. The bulky Cl^- ion pushes up on the L-cys molecule, skewing the transition dipole moment of the CS stretching mode away from a direction which is normal to the surface, thus decreasing the intensity of the SERS band. Upon desorption of the Cl^- the L-cys molecule will adopt a geometry whereby the C-S bond is normal to the surface and thus produces a larger SERS intensity.

Also of interest are the two peaks associated with the carboxyl group, the C_α-COO^- stretch at 898 cm^{-1} (Figure 3.8) and the COO^- stretch at 1396 cm^{-1} (Figure 3.9). The intensity of the C_α-COO^- peak follows a similar trend to the CS stretch, remaining constant when Cl^- is adsorbed, increasing in intensity once Cl^- desorption occurs. The higher frequency COO^- shows a more complicated relationship to potential. At more positive potentials the intensity of the peak still remains constant, however as the applied potential becomes more negative there is a sharp drop in intensity after Cl^- desorption begins to occur. The intensity then begins to climb once again.

When interpreting the trend of the 898 cm^{-1} peak it is reasonable to assume that the proximity to the surface will not play as big a role in the enhancement mechanism as the orientation of the transition dipole moment. Because this vibration is associated with the C_α-C stretching, whether the carboxyl group is pointing up or down will not greatly affect the distance from the surface, and thus the enhancement of the Raman band. The observed increase in intensity is therefore more likely to be

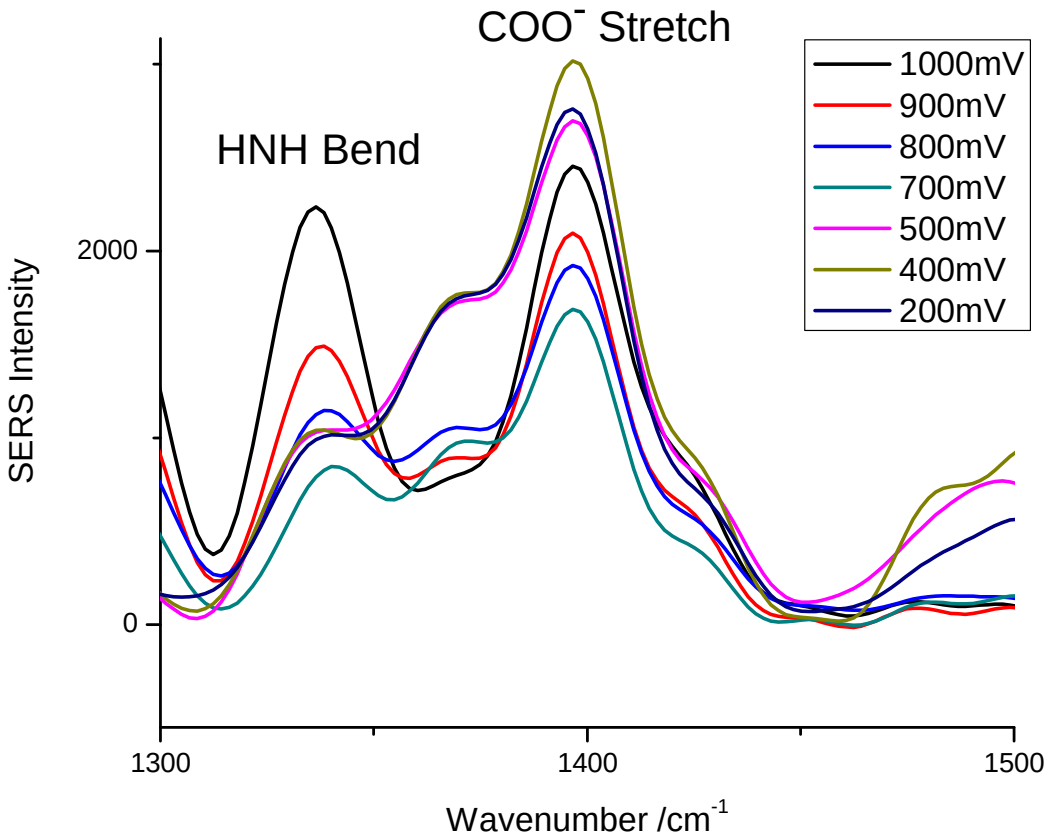

Figure 3.9 – HNH bending and COO^- stretching bands of SERS spectra of L-Cys adsorbed at a polycrystalline Ag electrode at selected potentials in 0.1M KCl, pH ≈6. All applied potentials are negative vs. Ag|AgCl.

attributed to the re-alignment of the transition dipole moment, becoming constantly more normal to the surface as the potential is made more negative.

The COO^- stretching band at 1396 cm^{-1}, however, appears to be affected by both proximity to the surface and the alignment of the transition dipole moment. Indeed it appears that they are at odds with each other as the potential is made more

negative. The initial drop in intensity of the band can be related to the carboxyl group moving away from the surface. The subsequent increase in the intensity of the band can then be attributed to the transition dipole moment of the vibration (which is similar to that of the 896 cm^{-1} band) becoming more normal to the surface as it re-orients to the Anti(II) configuration.

The only Raman band which provided any information related to the amino group was the HNH bend observed at 1338 cm^{-1}. This band was observed to remain constant for more positive potentials where Cl^- desorption did not occur. There is a slight drop in SERS intensity around where Cl^- desorption begins to occur, most likely due to the Cl^- stabilized amino complex being destabilized. The SERS intensity however does increase significantly after this initial drop as the potential is made more negative. This is consistent with the amino group interacting directly with the surface and not through the Cl^- ion. It is possible that this configurational change is also resulting in a more favourable orientation of the transition dipole moment, thus accounting for the large increase in the SERS intensity observed from this peak.

The driving forces of the proposed model are simple in concept, and can be understood from an electrostatic perspective. Applied potentials were varied from more positive to more negative. As previously stated, the pzc for polycrystalline Ag is -900 mV, thus, initially the electrode surface would be more positively charged. The negatively charged deprotonated carboxyl group will interact favourably with the positive surface, thus allowing the carboxylate group to be pointing down to the surface initially. The layer of adsorbed Cl^- will also allow for the positively charged

protonated amino group to be in close proximity to the surface. As the applied potential is made more negative, the surface will become more negatively charged, and the carboxyl group will be repelled from the surface. The Cl^- ions will desorb from the surface and the positively charged amino group will be able to interact strongly with the increasingly negatively charged surface, despite the loss of the Cl^- stabilization. Additionally, without the layer of Cl^- ions present at the surface the amino group will be able to get closer to the electrode surface, thus increasing the SERS enhancement of the HNH bending mode at 1338 cm^{-1}.

Also, since the amino group is no longer stabilized by the Cl^- ions the L-cys molecule is able to adopt a configuration where the C-S transition dipole moment is more normal to the surface. These mechanisms can account for all of the observed trends in the peak intensities of the *in situ* SERS spectra collected for L-cys on polycrystalline Ag under neutral pH conditions.

Acidic Conditions

In situ SERS spectra were also collected for L-cys adsorbed at polycrystalline Ag under acidic conditions. This change should have the effect of protonating the carboxyl group, thus removing the zwitterionic behaviour exhibited by the adsorbate.

A CV for L-cys adsorbed at polycrystalline Ag at pH = 2 was collected (Figure 3.10). The CV shows good correlation with that obtained under neutral conditions with the oxidation and cathodic damaging of the Ag surface occurring at potentials more positive than -200 mV and more negative than -1100 mV

respectively. There is an additional feature under acidic conditions however not found in neutral conditions. A cathodic peak is observed in the reverse scan at approximately -1000 mV. Due to the strong Ag-S linkage formed between L-cysteine and Ag, and the lack of a complementary anodic peak, it is unlikely that this feature is attributable to the desorption of L-cys from the electrode surface. The charge transfer associated with this peak is quite large compared to that attributed to the desorption of .a monolayer of L-cysteine from a Au(111) surface[73]. It is quite clear from these results that this could not simply be due to desorption of a monolayer of L-cys from the Ag surface as the charge transfer is approximately 30 times larger than that expected. More likely is that electrochemical decomposition of the L-cys molecules at the surface occurs.

This theory is further supported by the *in situ* SERS spectra collected. At potentials more negative than -700 mV an abrupt change in emerging trends in peak intensity is observed, most notably in the sharp decrease in the peak height of the C-S stretching band at 672cm^{-1}. This is evident from the plot of SERS spectra collected from acidic media shown in Figure 3.11. The potential range for which L-cys is stable when adsorbed on polycrystalline Ag is therefore narrower in acidic media than neutral media. The analysis of *in situ* SERS spectra collected in this study is therefore limited to applied potentials ranging from -200 mV to -700 mV. Despite the reduced potential range which can be studied under acidic conditions, some interesting conclusions can be made regarding the system.

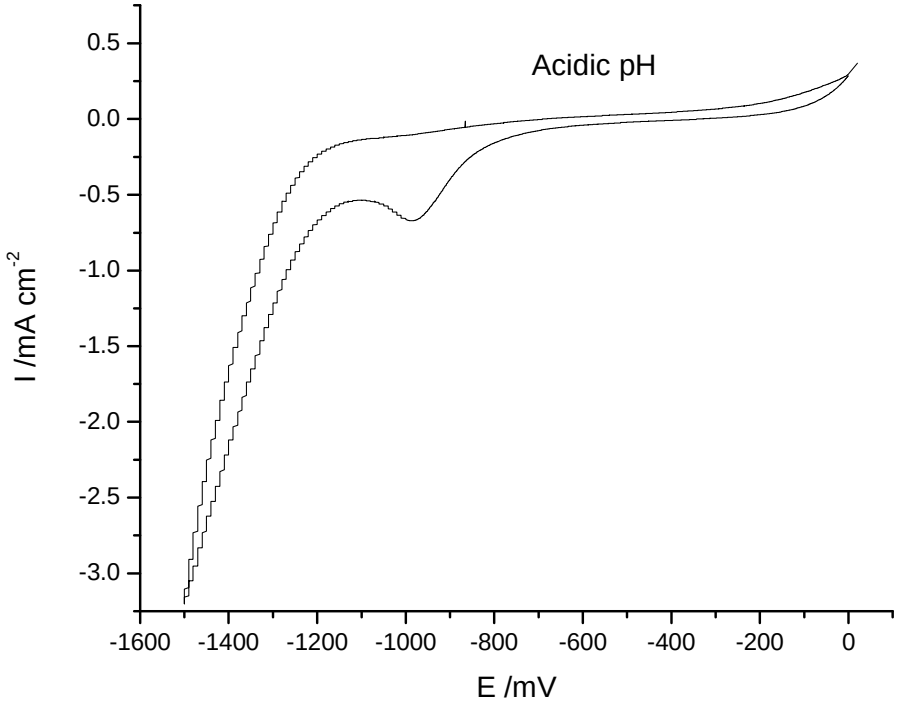

Figure 3.10 - Cyclic voltammogram of polycrystalline Ag in 0.1M L-Cys and 0.1M KCl acidified to pH = 2 as measured against a Ag|AgCl reference. Sweep rate = 40mV/s, 0.3mV steps in staircase potential ramp.

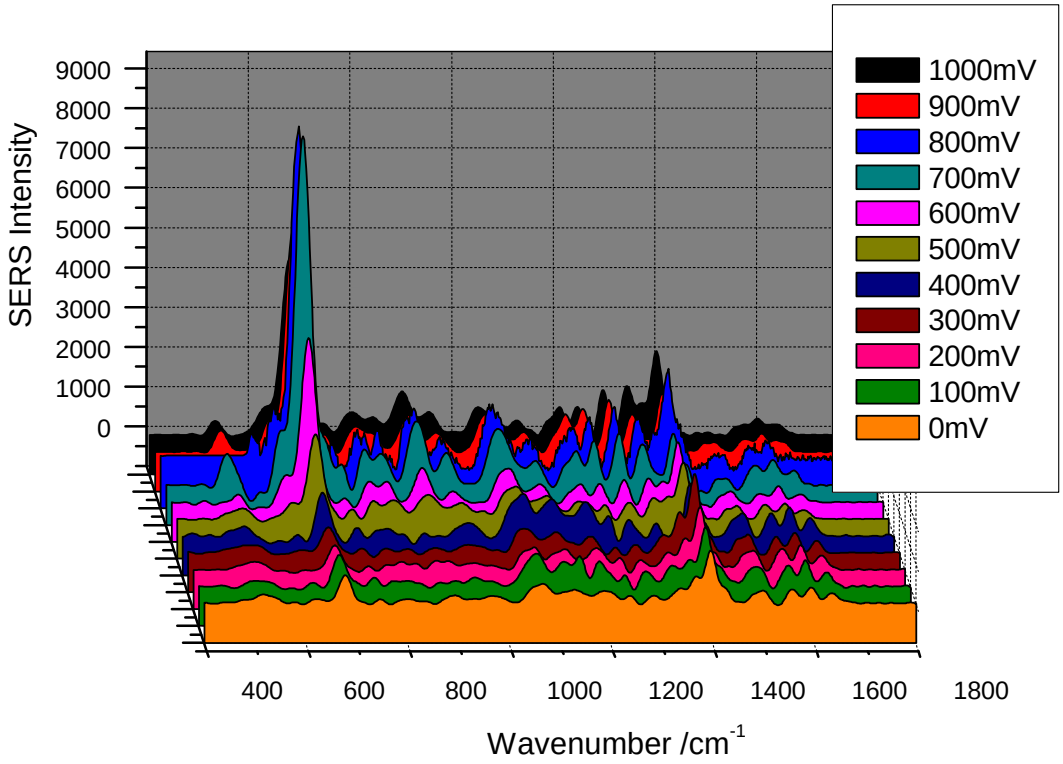

Figure 3.11 - *In situ* SERS spectra of L-Cys adsorbed at a polycrystalline Ag electrode in 0.1M KCl, acidified to pH =2.All applied potentials are negative vs. Ag|AgCl.

Most of the potential range analyzed in acidic electrolyte is more positive than the potential at which we expect to see the onset of Cl^- desorption. For this reason there is not much variation in peak intensity as the potential is made more negative. The proposed adsorption geometry of L-cys on polycrystalline Ag under acidic conditions is shown in neutral conditions, at more positive potentials the protonated amino group is stabilized by coadsorbed Cl^-.

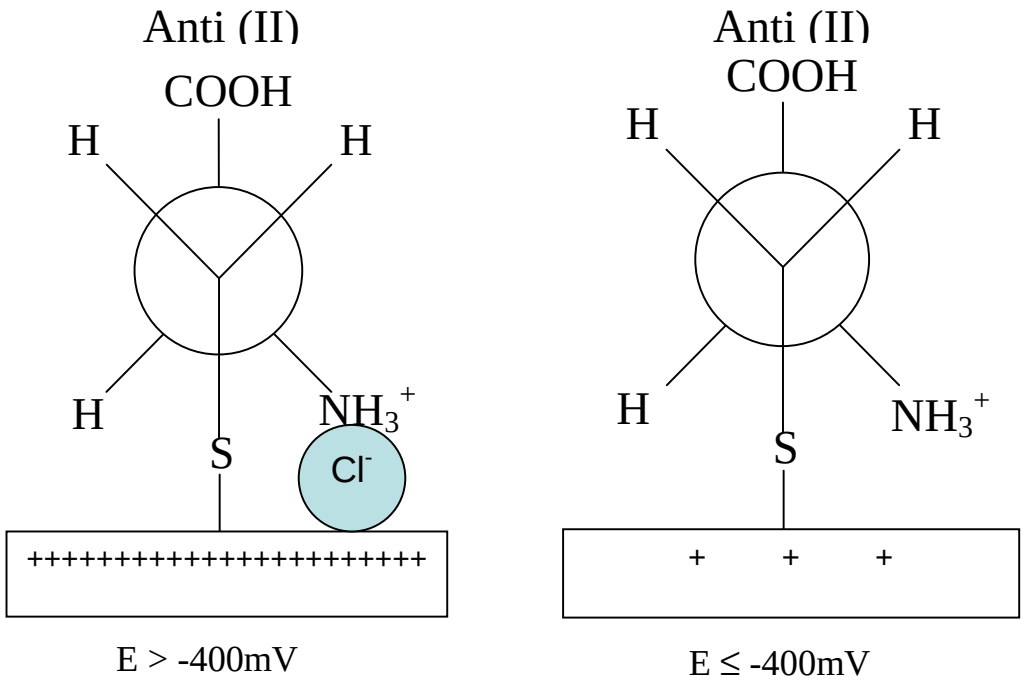

Figure 3.12 - Newman projections showing the adsorption geometry of L-cys on Ag in 0.1M KCl, acidified to pH = 2.

This again causes the C-S bond of the adsorbed L-cys molecules to be skewed away from normal to the surface. The main difference between the neutral and acidic conditions is the carboxylic group, which has no strong interaction with the electrode surface when protonated in acidic media. It is therefore not expected that applied potential will have a major influence on orientation of the carboxylic group.

An increase in the peak height of the C-S stretching mode is observed starting from -400 mV until the electrochemical decomposition of the adsorbate begins to occur at -800 mV (Figure 3.13). In neutral media the increase in intensity of the C-S stretching mode coincided with the desorption of Cl^- from the electrode surface,

prompting a re-orientation of the L-cys. A similar argument can be made with the acidic system. This increase is observed at potentials more positive than where Cl^- desorption is expected to occur however. This could indicate two different things. First of all it is possible that Cl^- desorption would occur at a more positive potential in acidic media, and thus the intensity increases observed are consistent with Cl^- desorption from the electrode surface. Therefore as the applied potential is made more negative the Cl^- desorbs and the L-cys molecules consequently adopt a geometry whereby the transition dipole moment for the C-S stretching mode is more normal to the electrode surface. The desorption of Cl^- occurring at more positive potentials in acidic media compared to neutral would be most likely to occur as a result of a combination of two factors. Firstly a pseudo-reference electrode was used, and thus has a non-standardized response. The difference in pH and concentration of the electrolytes would almost certainly result in a discrepancy between the measured and actual potential of the cell. Secondly, it is possible that the pzc of the Ag electrode would have shifted to a more positive potential in acidic media, due to the increased positive charge near the surface due to hydronium ions. The other possibility is that, because the carboxyl group is no longer strongly interacting with the electrode surface it is easier for the adsorbed L-cys molecules to re-orient, despite the Cl^- stabilized amino group interaction.

Further analysis of the entire frequency range of the SERS spectra collected supports the former hypothesis. The additional peaks of interest are the C_α-COOH stretching mode at 894 cm^{-1}, the COOH stretching mode at 1398 $cm^{-1}$and the HNH bending mode at 1338 cm^{-1}.

As discussed above, the enhancement of the C_α-COOH stretching mode can be mainly attributed to the orientation of the transition dipole moment of the vibration. The desorption of the coadsorbed Cl^- should result in the straightening of the entire L-cys molecule. This would translate the transition dipole moment of the C_α-COOH vibration from skewed to more normal to the surface, thus increasing the SERS enhancement observed by this vibrational mode.

There is no meaningful change in the intensity of the COOH stretching mode at 1398 cm^{-1}. This is not surprising, as there is no major change in the orientation of the carboxyl group as the potential is varied. The adsorbed L-cys molecules will go from a skewed orientation to one more normal to the surface, while the rotamer is the same regardless of potential. There are only minor influences on this band which would be in effect. As the potential is scanned cathodically a slight increase in the SERS enhancement could be expected from the re-alignment of the transition dipole moment. However the straightening of the L-cys molecule would also result in the carboxylic group moving further away from the surface. The data shown in Figure 3.14 shows that these opposing forces effectively cancel each other out, resulting in no overall improvement in the SERS enhancement of the COOH stretching mode as the potential is made more negative.

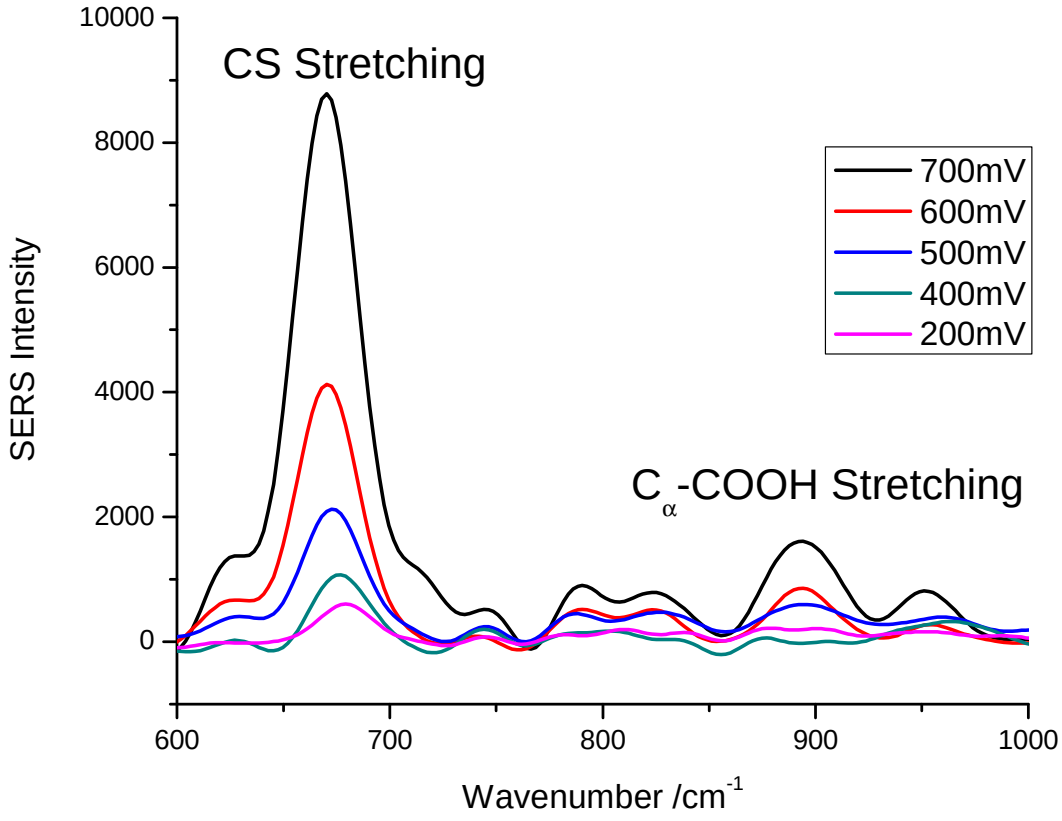

Figure 3.13 – CS and C_α-COOH stretching bands of SERS spectra of L-cys adsorbed at a polycrystalline Ag electrode at selected potentials in 0.1M KCl acidified to pH=2. All applied potentials are negative vs. Ag|AgCl.

The HNH bending mode at 1338 cm^{-1} also supports the adsorption geometry depicted in Figure 3.12. At potentials more negative than -300 mV the peak becomes larger and more well-defined. Cl^- adsorbed on the electrode surface at more positive potentials will shield the amino group from the local electromagnetic field. The stabilization of the amino group by the coadsorbed Cl^- ions will also keep the amino group from interacting directly with the surface. Once the Cl^- starts to desorb from the surface we would therefore expect to see an increase in the SERS enhancement of the

HNH bending mode due to the closer proximity of the amino group to the surface and the reduced shielding by the coadsorbed Cl^- ions.

The adsorption geometry proposed for L-cys on a polycrystalline Ag surface under acidic conditions can be explained using the same principles as for neutral pH conditions. The protonated amino group is positively charged, thereby interacting with the coadsorbed Cl^- ions. As the applied potentials negatively charge the electrode surface the Cl^- ions are desorbed, allowing the positively charged amino group to interact with the increasingly negatively charged metal surface. The carboxylic group in its protonated form is not charged, and therefore is not directly affected by the change in charge density of the electrode. Therefore as the applied potential is made more negative no conversion between rotamers of L-cys occurs.

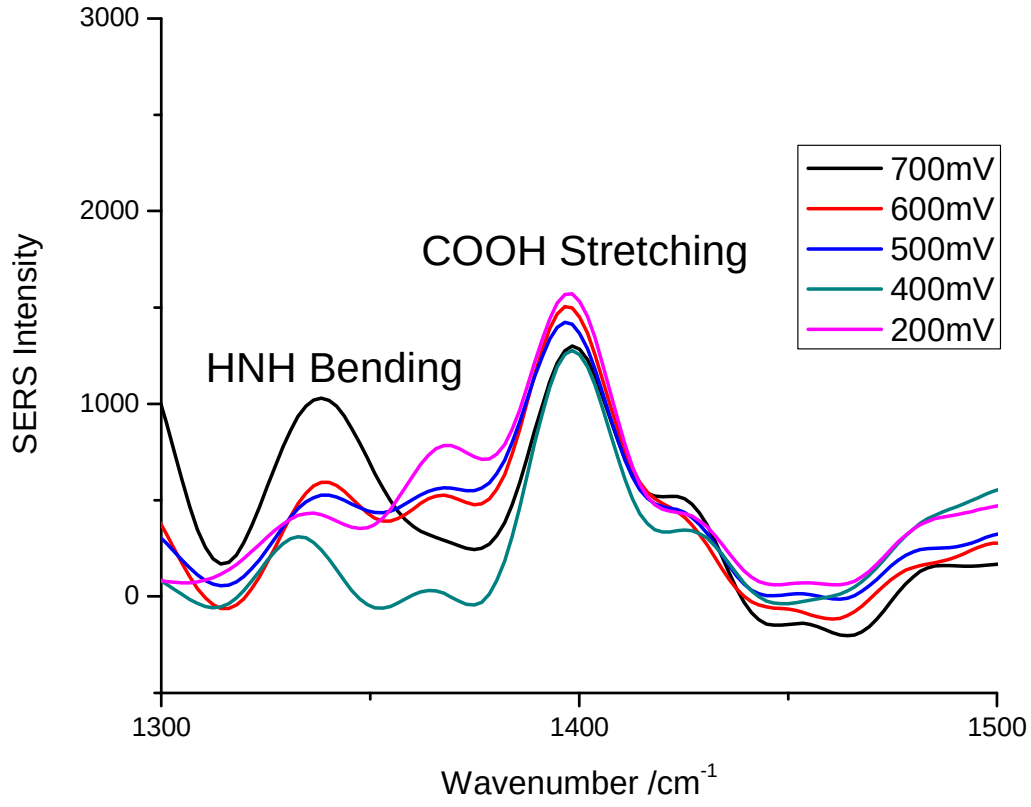

Figure 3.14 – HNH bending and COOH stretching bands of SERS spectra of L-Cys adsorbed at a polycrystalline Ag electrode at selected potentials in 0.1M KCl acidified to pH=2. All applied potentials are negative vs. Ag|AgCl.

3.4 Summary and Conclusions

The aim of the experiments discussed in this chapter was to gain insight into the adsorption of L-cys on a polycrystalline Ag electrode under different pH conditions as a function of applied potential. Assignment of Raman bands for L-cys in aqueous media at acidic, neutral and basic pH was completed using DFT calculations and comparison to literature sources. This resulted in the assignment of

all major peaks in the Raman spectrum of L-cys. This also confirmed that the protonation state of the L-cys molecule has a small, but measureable effect on certain vibrational modes in the solution Raman spectrum.

In situ SERS experiments were then performed on a polycrystalline Ag electrode with L-cys adsorbed under different pH conditions. To ensure that the adsorbed L-cys was not being damaged electrochemically over the potential range studied in SERS experiments CV experiments were also performed. Using the band assignment the vibrational modes which showed indicative increases and decreases in peak intensities with the applied potential were correlated with certain functional groups in the L-cysteine molecule and their adsorption geometry. From these observations it was determined that in neutral electrolyte L-cys switches from a Gauche configuration with the amino group stabilized by coadsorbed Cl^- at more positive applied potentials. The Cl^- stabilization also causes the L-cys to adsorb in a skewed manner, whereby the C-S bond is deviated away from an angle normal to the surface. As the applied potential is made more negative the Cl^- desorbs from the surface and the adsorbed L-cys is converted to the Anti(II) rotamer while also straightening out into an adsorption geometry more normal to the electrode surface.

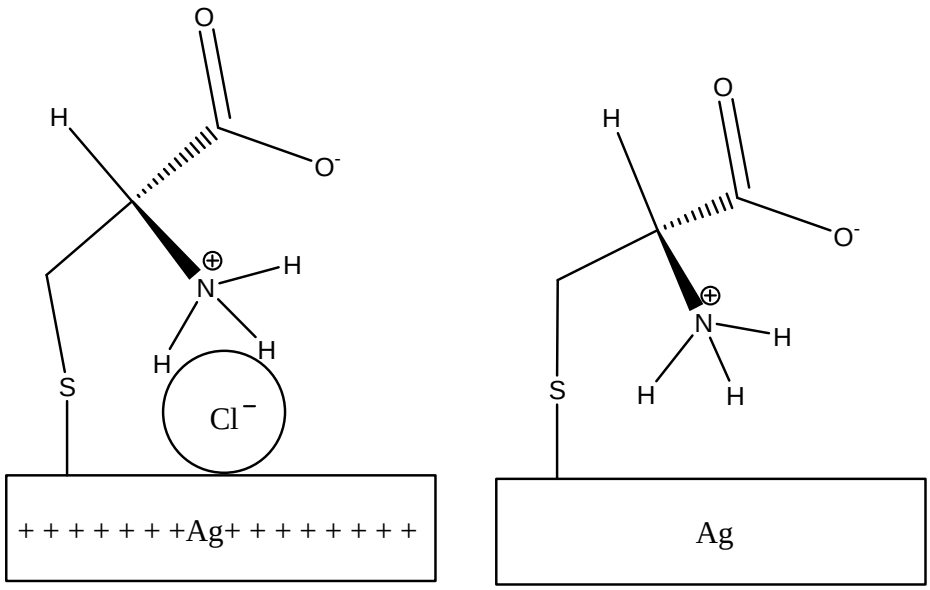

(a) (b)

Figure 3.15 – Schematic illustrating the skewing of the C-S bond in L-cysteine adsorbed on Ag, as a result of interaction with coadsorbed Cl^- ions.

In acidic electrolyte electrochemical decomposition was observed at potentials more negative than -800 mV in the CVs which were collected, thereby decreasing the potential range studied in acidic media. From the *in* situ SERS spectra collected in the "safe" potential range it was determined that L-cys adsorbs onto polycrystalline Ag in an Anti(II) configuration at more positive potentials. As with adsorption under neutral conditions, the amino group was stabilized by the coadsorbed Cl^- ions, similarly skewing the L-cysteine molecule away from a more perpendicular adsorption geometry. As the potential was made more negative the Cl^- ions desorbed from the electrode surface at a more positive potential than under neutral conditions. Unlike in neutral electrolyte however, the desorption of the coadsorbed Cl^- did not result in a change to a different rotamer. An Anti(II) configuration was determined to still be

dominant, with the only change being a straightening of the L-cys molecule towards a more perpendicular adsorption geometry.

The SERS experiments conducted under basic conditions require further exploration to definitively interpret the results. There are some unexpected bands, not present in either neutral or acidic media which still need to be identified. It is possible that a decomposition mechanism is responsible for these anomalies. Hydroxide adsorption is also likely to be a contributing factor in these results

This study was successful in presenting a model for the interaction of L-cys with a polycrystalline Ag electrode under potential and pH control. This has shown *in situ* SERS to be a powerful tool in the elucidation of surface binding characteristics of an adsorbate. These adsorption geometries were assigned based on the assumption that the electromagnetic mechanism of SERS enhancement was the main component of the observed changes in peak intensity. A further investigation into whether a CT mechanism may have also been contributing to the enhancement would lend strong support to the results already obtained, as would further experiments to clarify the behaviour of the system of interest under basic conditions.

Chapter 4 - Summary of SERS and SHG-ORD Results

In Chapters 2 and 3 it has been shown that a great deal of information can be collected regarding a system consisting of cysteine adsorbed on Ag probed *in situ* by SERS and SHG-ORD. Further insights can also be attained by considering the results from both sets of experiments.

From the SERS experiments conducted it was shown that in neutral media at applied potentials where Cl^- is adsorbed on the electrode surface a Gauche configuration where the protonated amino and deprotonated carboxylate groups are oriented down towards the Ag surface (see Figure 3.7) occurs. At more negative potentials, when the Cl^- begins to desorb from the electrode surface, an orientation change to an Anti(II) configuration where the carboxylate group is rotated away from the surface results. It is likely that these same trends would be observed for both the D and D,L forms of cysteine as well.

SHG-ORD studies performed show an interesting result when comparing rotational angle ϕ to the applied potential. There are two trends which can be observed in Figure 2.10. Firstly it is noticed that at more negative potentials the error associated with the rotation angles measured is smaller than at more positive potentials. Secondly, it appears that the magnitude of ϕ is greater at more positive potentials compared to more negative potentials.

The trends in the SHG-ORD experiments can be correlated with the processes observed in the SERS experiments. In section 2.1 the adsorption geometry requirements, as described by Kadodwala *et. al* were discussed[60,62]. They indicated that the instilling of optical activity from a chiral adsorbate onto the electronic structure of a metal requires that the adsorbate have a particular adsorption geometry, described as a chiral footprint. This chiral footprint indicates that the adsorbate is either interacting with the metal surface with three chiral groups, or that the overlayer structure of the adsorbed molecules is such that the adsorbate can impart chirality to the substrate.

As previously discussed in Chapter 2, the greater error at more positive potentials in SHG-ORD studies can be attributed to the coadsorption of Cl^-. It is likely that the Cl^- would interfere with the ability of cysteine to imprint its optical activity onto the electronic structure of the Ag, thus causing more variability in the measurement of ϕ.

The requirements described by Kadodwala *et. al* for the observation of optical activity from a metal indicate that a change in adsorption geometry, such as that observed, would likely result in a change in ϕ. The greater magnitude of ϕ at more positive potentials could therefore be linked to a stronger interaction between the cysteine and the Ag surface in the Gauche configuration compared to the Anti(II) configuration. This is a reasonable assertion as it would be expected that the carboxylate group would interact more strongly with the Ag surface than the hydrogen group would.

The complementary nature of *in situ* SHG-ORD and SERS is clearly demonstrated through the experiments performed and their interpretation. An intriguing combination of information regarding electrochemical behaviour, adsorption geometry, adsorption strength and instillation of optical activity from adsorbate to substrate can be collected. These studies can lead to inferences not otherwise attainable which could have many interesting applications.

References

(1) Tengvall, P.; Lestelius, M.; Liedberg, B.; Lundstroem, I. *Langmuir* **2002**, *8*, 1236.

(2) O'Neil, M. J.; Smith, A.; Heekelman, P. E.; Obenchain Jr., J. R.; Gallipeau, J. A. R.; D'Arecca, M. A.; Budavari, S. The Merck Index: An Index of Chemical, Drugs and Biologicals; 13 ed.; Merck & Co., Inc.: Whitehouse Station, NJ, 2001; pp 486.

(3) Matos, J. B.; Pereira, L. P.; Agostinho, S. M. L.; Barcia, O. E.; Cordeiro, G. G. O.; D'Elia, E. *Journal of Electroanalytical Chemistry* **2004**, *570*, 91.

(4) Martens, J.; Offermanns, H.; Scherberich, P. *Angewandte Chemie-International Edition in English* **1981**, *20*, 668.

(5) Ralph, T. R.; Hitchman, M. L.; Millington, J. P.; Walsh, F. C. *Journal of Electroanalytical Chemistry* **1994**, *375*, 17.

(6) Liu, A.-C.; Chen, D.-c.; Lin, C.-C.; Chou, H.-H.; Chen, C.-h. *Analytical Chemistry* **1999**, *71*, 1549.

(7) Ismail, K. A. *Electrochimica Acta* **2007**, *52*, 7811.

(8) Sanders, D. R. Material Safety Data Sheet; Benzotriazole, 2006.

(9) Da-Quan, Z.; Li-Xin, G.; Guo-Ding, Z. *Journal of Applied Electrochemistry* **2005**, *35*, 1081.

(10) Watanabe, T.; Maeda, H. *Journal of Physical Chemistry* **1989**, *93*, 3258.

(11) Brolo, A. G.; Germain, P.; Hager, G. *Journal of Physical Chemistry B* **2002**, *106*, 5982.

(12) Paik, W. K.; Eu, S.; Lee, K.; Chon, S.; Kim, M. *Langmuir* **2000**, *16*, 10198.

(13) Campagnola, P. J.; Wei, M.-d.; Lewis, A.; Loew, L. M. *Biophysics Journal* **1999**, *77*, 3341.

(14) Corn, R. M.; Higgins, D. A. *Chemical Reviews* **1994**, *94*, 107.

(15) Brevet, P.-F. *Surface Second Harmonic Generation*; Presses polytechniques et universitaires romandes: Lausanne, 1997.

(16) Pettinger, B.; Bilger, C.; Lipkowski, J.; Schmickler, W. Second Harmonic Generation Anisotropy from Single Crystalline Electrode Surfaces. In *Interfacial Electrochemistry: Theory, Experiment, and Applications*; Wieckowski, A., Ed.; Marcel Dekker, Inc.: New York, 1999; pp 373.

(17) Richmond, G. L.; Robinson, J. M.; Shannon, V. L. *Progress in Surface Science* **1988**, *28*, 1.

(18) Guyot-Sionnest, P.; Tadjeddine, A. *Journal of Chemical Physics* **1990**, *92*, 734.

(19) Raman, C. V.; Krishnan, K. S. *Nature* **1928**, *121*, 501.

(20) Clark, R. J. H.; Hester, R. E. *Advances in Infrared and Raman Spectroscopy*; Heyden & Son Ltd.: New York, 1975; Vol. 1.

(21) McCreery, R. L. *Raman Spectroscopy for Chemical Analysis*; John Wiley & Sons, Inc.: Toronto, 2000; Vol. 157.

(22) Stoicheff, B. P. High Resolution Raman Spectroscopy. In *Advances in Spectroscopy*; Thompson, H. W., Ed.; Interscience Publishers Ltd.: New York, 1959; Vol. 1; pp 91.

(23) Szymanski, H. A. *Raman Spectroscopy: Theory and Practice*; Plenum Press: New York, 1967; Vol. 1.

(24) Szymanski, H. A. *Raman Spectroscopy: Theory and Practice*; Plenum Press: New York, 1970; Vol. 2.

(25) Hexter, R. M.; Albrecht, M. G. *Spectrochimica Acta Part a-Molecular and Biomolecular Spectroscopy* **1979**, *35*, 233.

(26) Long, D. A. *Chemistry in Britain* **1989**, *6*, 592.

(27) Sanderson, A. C. Surface-enhanced Raman scattering from a modified silver electrode, University of Victoria, 2007.

(28) Fleischmann, M.; Hendra, P. J.; McQuillan, A. J. *Chemical Physics Letters* **1974**, *26*, 163.

(29) Jeanmaire, D. L.; Van Duyne, R. P. *Journal of Electroanalytical Chemistry* **1977**, *84*, 1.

(30) Albrecht, M. G.; Creighton, J. A. *Jounral of the Amercian Chemical Society* **1977**, *99*, 5215.

(31) Kneipp, K.; Kneipp, H.; Itzkan, I.; Dasari, R. R.; Feld, M. S. *Journal of Physics: Condensed Matter* **2002**, *14*, R597.

(32) Barnes, W. L.; Dereux, A.; Ebbesen, T. W. *Nature* **2003**, *424*, 824.

(33) Pettinger, B. In situ Raman spectroscopy at metal electrodes. In *Adsorption of Molecules at Metal Electrodes*; Lipkowski, J., Ross, P. N., Eds.; VCH: New York, 1992; pp 285.

(34) Kerker, M. *Accounts of Chemical Research* **1984**, *17*, 271.

(35) Kerker, M.; Wang, D. S.; Chew, H. *Applied Optics* **1980**, *19*, 4159.

(36) Brolo, A. G. Surface-Enhanced Raman Scattering (SERS) Studies of Pyrazine Adsorbed on Polycrystalline and Single Crystal Electrodes., University of Waterloo, 1998.

(37) Albano, E. V.; Daiser, S.; Ertl, G.; Miranda, R.; Wandelt, K.; Garcia, N. *Physical Review Letters* **1983**, *51*, 2314.

(38) García-Vidal, F. J.; Pendry, J. B. *Physical Review Letters* **1996**, *77*, 1163.

(39) Xu, M.; Dignam, M. J. *The Journal of Chemical Physics* **1992**, *96*, 7758.

(40) Xu, H.; Aizpurua, J.; Käll, M.; Apell, P. *Physical Review E* **2000**, *62*, 4318.

(41) Kneipp, J.; Kneipp, H.; Kneipp, K. *Chemical Society Reviews* **2008**, *37*, 1052.

(42) Kneipp, K.; Wang, Y.; Kneipp, H.; Perelman, L. T.; Itzkan, I.; Dasari, R. R.; Feld, M. S. *Physical Review Letters* **1997**, *78*, 1667.

(43) Pieczonka, N. P. W.; Aroca, R. F. *Chemical Society Reviews* **2008**, *37*, 946.

(44) Qian, X. M.; Nie, S. M. *Chemical Society Reviews* **2008**, *37*, 912.

(45) Otto, A. *Journal of Raman Spectroscopy* **1991**, *22*, 743.

(46) Otto, A.; Mrozek, I.; Grabhorn, H.; Akemann, W. *Journal of Physics: Condensed Matter* **1992**, *4*, 1143.

(47) Otto, A.; Timper, J.; Billmann, J.; Kovacs, G.; Pockrand, I. *Surface Science* **1980**, *92*, L55.

(48) Lombardi, J. R.; Birke, R. L.; Lu, T.; Xu, J. *The Journal of Chemical Physics* **1986**, *84*, 4174.

(49) Koch, W.; Holthausen, M. C. *A Chemist's Guide to Density Functional Theory*, 2nd ed.; Wiley-VCH Verlag: Germany, 2000.

(50) Seminario, J. M. An introduction to density functional theory in chemistry. In *Modern Density Functional Theory: A Tool for Chemistry*; Seminario, J. M., Politzer, P., Eds.; Elsevier: New York, 1995; pp 418.

(51) Hartree, D. R. *Mathematical Proceedings of the Cambridge Philosophical Society* **1928**, *24*, 89.

(52) Fock, V. *Zeitschrift fur Physik* **1930**, *61*, 126.

(53) Boys, S. F. *Proceedings of the Royal Society of London. Series A. Mathematical and Physical Sciences* **1950**, *200*, 542.

(54) Hohenberg, P.; Kohn, W. *Physical Review* **1964**, *136*, B864.

(55) Kohn, W.; Sham, L. J. *Physical Review* **1965**, *140*, A1133.

(56) Belkin, M. A.; Shen, Y. R. *International Reviews in Physical Chemistry* **2005**, *24*, 257.

(57) Byers, J. D.; Yee, H. I.; Hicks, J. M. *The Journal of Chemical Physics* **1994**, *101*, 6233.

(58) Verbiest, T.; Kauranen, M.; Persoons, A. *Journal of Materials Chemistry* **1999**, *9*, 2005.

(59) Schanne-Klein, M. C.; Hache, F.; Roy, A.; Flytzanis, C.; Payrastre, C. *The Journal of Chemical Physics* **1998**, *108*, 9436.

(60) Bovet, N.; McMillan, N.; Gadegaard, N.; Kadodwala, M. *The Journal of Physical Chemistry B* **2007**, *111*, 10005.

(61) Mulligan, A.; Lane, I.; Rousseau, G. B. D.; Johnston, S. M.; Lennon, D.; Kadodwala, M. *Angewandte Chemie International Edition* **2005**, *44*, 1830.

(62) Mulligan, A.; Lane, I.; Rousseau, G. B. D.; Johnston, S. M.; Lennon, D.; Kadodwala, M. *Journal of Physical Chemistry B* **2006**, *110*, 1083.

(63) Koechner, W. Optical Pump Systems. In *Solid-State Laser Engineering*; 3 ed.; Schawlow, A. L., Shimoda, K., Siegman, A. E., Tamir, T., Eds.; Springer-Verlag: New York, 1992; Vol. 1; pp 275.

(64) Li, H.; Wurrey, C. J.; Thomas, G. J. *Journal of the American Chemical Society* **1992**, *114*, 7463.

(65) Pawlukojc, A.; Leciejewicz, J.; Ramirez-Cuesta, A. J.; Nowicka-Scheibe, J. *Spectrochimica Acta Part A: Molecular and Biomolecular Spectroscopy* **2005**, *61*, 2474.

(66) Madec, C.; Lauransan, J.; Garrigou-Lagrange, C. *Canadian Journal of Spectroscopy* **1980**, *25*, 47.

(67) Tarakeshwar, P.; Manogaran, S. *Spectrochimica Acta Part A: Molecular and Biomolecular Spectroscopy* **1995**, *51*, 925.

(68) Jing, C. Y.; Fang, Y. *Chemical Physics* **2007**, *332*, 27.

(69) Graff, M.; Bukowska, J. *Journal of Physical Chemistry B* **2005**, *109*, 9567.

(70) Campion, A.; Kambhampati, P. *Chemical Society Reviews* **1998**, *27*, 241.

(71) Moskovits, M. *Reviews of Modern Physics* **1985**, *57*, 783.
(72) Moskovits, M. *Journal of Raman Spectroscopy* **2005**, *36*, 485.
(73) Hager, G.; Brolo, A. G. *Journal of Electroanalytical Chemistry* **2003**, *550-551*, 291.

Appendix A

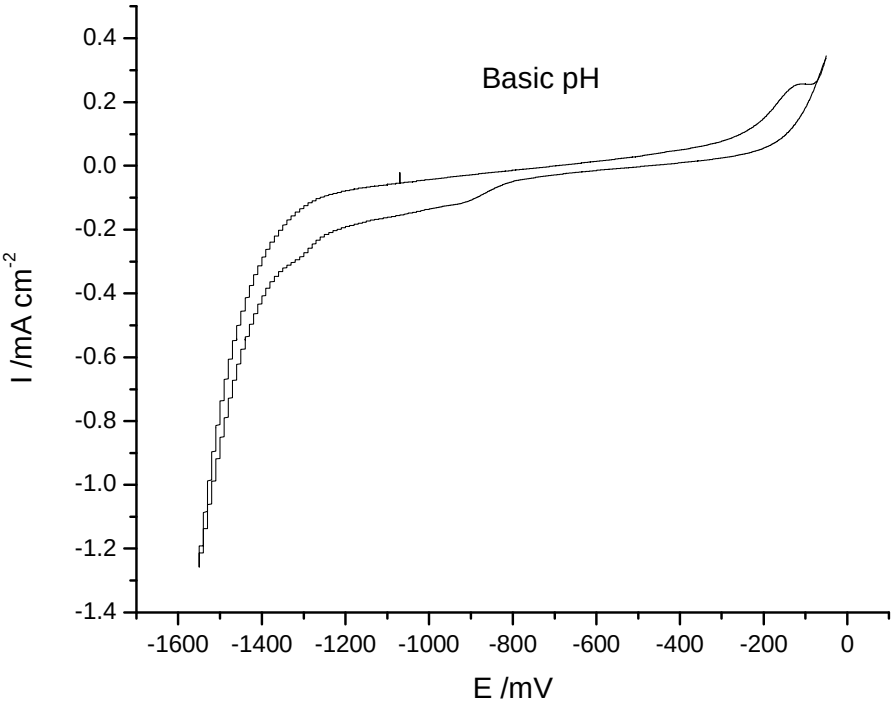

Cyclic voltammogram of polycrystalline Ag in 0.1M L-Cys and 0.1M NaOH, pH = 13. Potentials measured vs. pseudo Ag|AgCl reference.

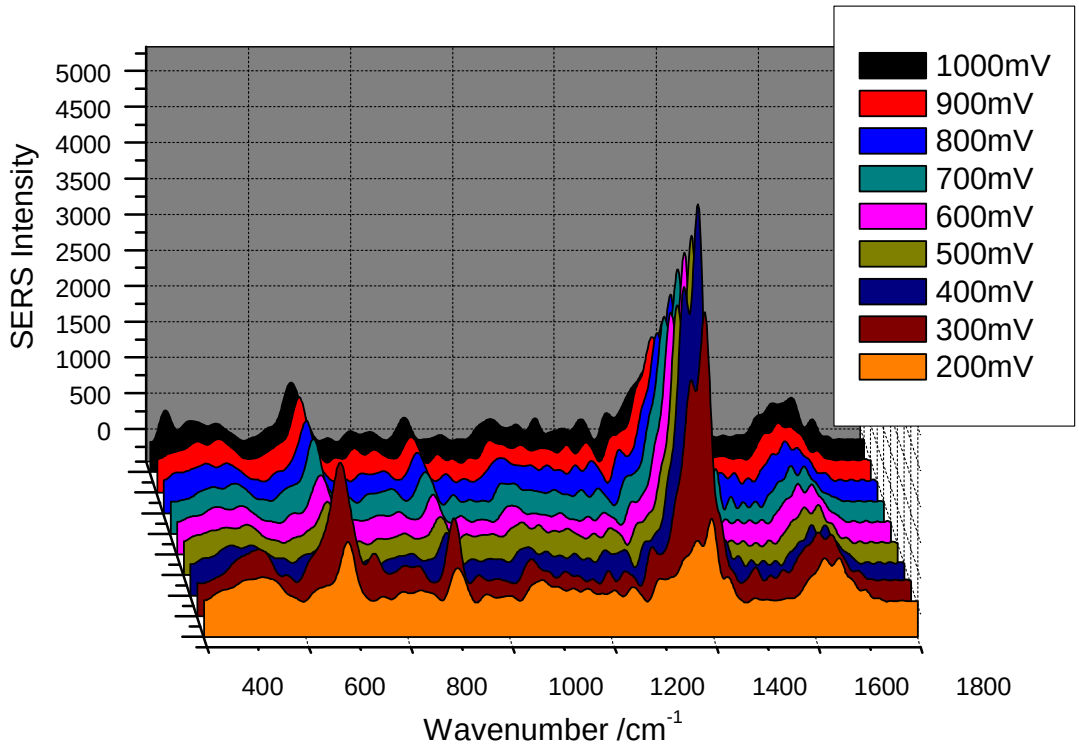

In situ SERS spectra of L-Cys adsorbed at a polycrystalline Ag electrode in 0.1M NaOH, pH = 13..All applied potentials are negative vs. pseudo Ag|AgCl.

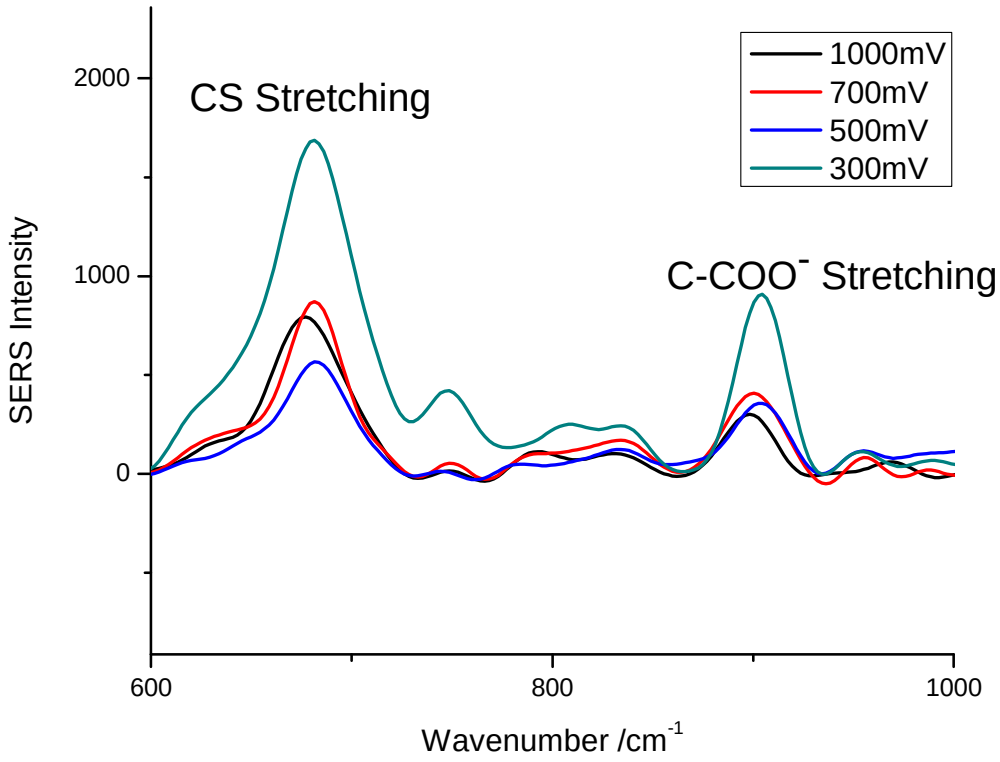

CS and C_{α}-COO^{-} stretching bands of SERS spectra of L-Cys adsorbed at a polycrystalline Ag electrode in 0.1M NaOH, pH =13. All applied potentials are negative vs. pseudo Ag|AgCl.

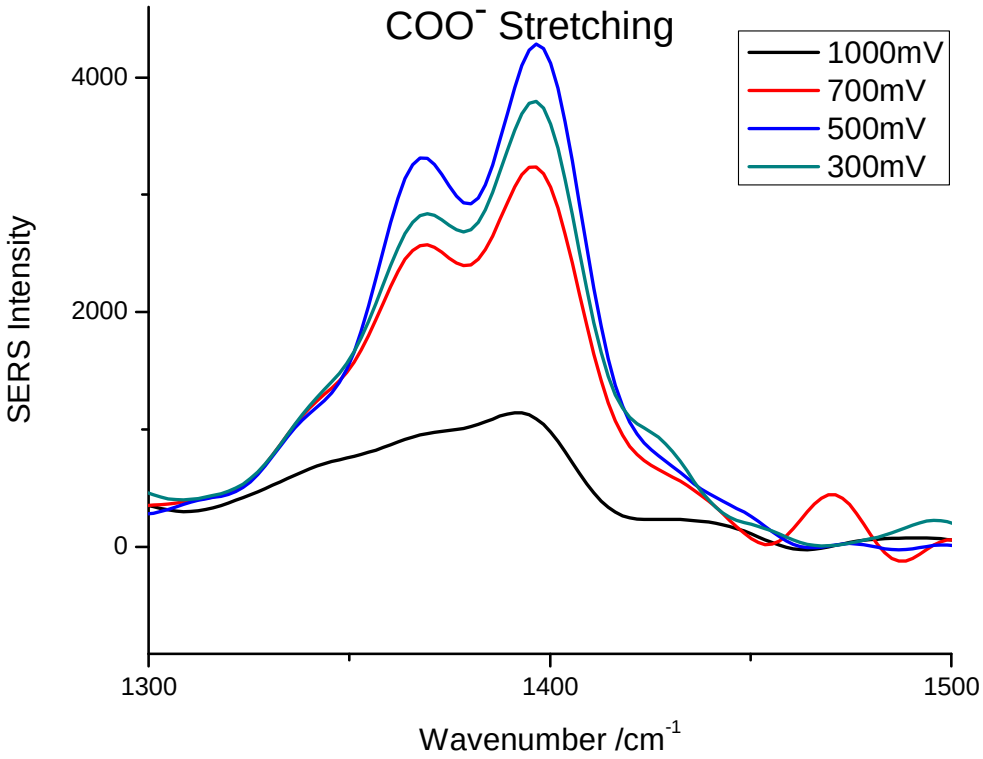

COO^- stretching bands of SERS spectra of L-Cys adsorbed at a polycrystalline Ag electrode in 0.1M NaOH, pH =13. All applied potentials are negative vs. pseudo Ag|AgCl.